contents is not expected.[16] In addition, the case-control study, which uses patient of other nervous diseases with dementia as a control, is not suitable to evaluate the risk of aluminum that is neurotoxic. So far the results of the epidemiological research has been consistent with the hypothesis that aluminum is one of the risk factors for the senile dementia of Alzheimer's type. Therefore, it is probable that aluminum is an environmental factor responsible for sporadic Alzheimer's disease of which the cause has not been specified yet. Because genetic research is advancing rapidly, an unknown factor may soon be clarified. However, at the present time it is believed that several factors participate in the etiology of sporadic Alzheimer's disease such as aging. There is a need to increase research efforts to reveal the cause of sporadic Alzheimer's disease. If the environmental factor is clarified, the incidence of the disease will be decreased when it is avoided. It has been shown that nerve cells are widely damaged at the onset of the symptom of senile dementia. It is therefore necessary to find the changes in the nerve cells caused by a specific environmental factor as early as possible. Thus the development of an early diagnostic method is very imperative. Such a method can be applied for screening purposes as health examinations. The recovery from, or prevention of aggravation of the disease is possible by early diagnosis and the early treatment.

The epidemiological survey of Alzheimer's disease and aluminum in drinking water described here has not been performed in Japan, where high concentrations of aluminum are observed in underground water, fountain water, mineral springs, and hot springs with various minerals. Therefore, necessary attention should be paid to the contents of aluminum in drinking water. In conclusion, it is important to advance research to specify the environmental factor in the cause of Alzheimer's disease further and to prescribe a preventive method.

References

1. McLachlan DRC. Aluminium and the risk for Alzheimer's disease. Environmetrics 1995; 6: 233–275.
2. Morishima-Kawashima M, Ihara Y. Recent advances in Alzheimer's disease. Seikagaku 2001; 73: 1297–1307. (in Japanese)
3. Klatzo I, Wisniewski H, Streicher E. Experimental production of neurofibrillary degeneration. J Neuropathol Exp Neurol 1965; 24: 187–199.
4. Alfrey AC, LeGendre GR, Kaehny WD. The dialysis encephalopathy syndrome: possible aluminum intoxication. N Engl J Med 1976; 294: 184–188.
5. Scholtz CL, Swash M, Gray A, Kogeorgos J, Marsh F. Neurofibrillary neuronal degeneration in dialysis dementia: a feature of aluminum toxicity. Clin Neuropathol 1987; 6 : 93–97.
6. Hulley SB, Cummings SR, Designing Clinical Research. An Epidemiologic Approach, Williams & Wilkins, Baltimore, 1988.
7. Vogt T. Water quality and health: study of a possible relation between aluminium in drinking water and dementia. Central Bureau of statistics, Oslo, 1986. (Sosiale og Okonomiske Studier, 61: 1–99.) (in Norwegian with English abstract)
8. FlatenTP. Geographical associations between aluminium in drinking water and death rates with dementia (including Alzheimer's disease), Parkinson's and Amyotrophic lateral sclerosis in Norway. Trace Elem Med 1987; 4: 179–180.
9. Frecker MF. Dementia in Newfoundland: identification of a geographical isolate? J Epidemiol Community Health 1991; 45: 307–311.
10. Neri LC. Hewitt D. Aluminium, Alzheimer's disease, and drinking water. Lancet 1991; 338: 390.
11. McLachlan DRC, Bergeron C, Smith JE, Boomer D, Rifat SL. Risk for neuropathologically confirmed Alzheimer's disease and residual aluminum in municipal drinking water employing weighted residential histories. Neurology 1996; 46: 401–405.
12. Gauthier E, Fortier I, Courchesne F, et al. Aluminum forms in drinking water and risk of Alzheimer's disease. Environ Res 2000; 84: 234–246.
13. Martyn CN, Barker DJP, Osmond C, et al. Geographical relation between Alzheimer's disease and aluminium in drinking water. Lancet 1989; 1: 59–62.
14. Martyn CN, Coggon DN, Inskip H, Lacey RF, Young WF. Aluminum concentrations in drinking water and risk of Alzheimer's disease. Epidemiology 1997; 8: 281-286.
15. Forster DP, Newens AJ, Kay DWK, Edwardson JA, Risk factors in clinically diagnosed presenile dementia of the Alzheimer type: a case-control study in northern England. J Epidemiol Community Health 1995; 49: 253–258.
16. Wettstein A, Aeppli J, Gautschi K, Peters M. Failure to find a relationship between domestic skills of octogenarians and aluminum in drinking water. Int Arch Occup Environ Health 1991; 63: 97–103.
17. Forbes WF, Hayward LM, Agwani N. Dementia, aluminium, and fluoride. Lancet 1991; 338: 1592–1593.
18. Jacqmin H, Commenges D, Letenneur L, Barberger-Gateau P, Dartigues, JF. Components of drinking water and risk of cognitive impairment in the elderly. Am J Epidemiol 1994; 139: 48–57.
19. Rondeau V, Commenges D, Jacqmin-Gadda H, Dartigues, JF. Relation between aluminum concentrations in drinking water and Alzheimer's disease: an 8-year follow-up study. Am J Epidemiol 2000; 152: 59–66.
20. Forbes WF, Agwani N. A suggested mechanism for aluminum biotoxicity. J Theor Biol 1994; 171: 207–214.
21. Meshitsuka M, Inoue M, Urinary excretion of aluminum from antacid ingestion and estimation of its apparent biological half-time. Trace Elem Electrolyts 1998; 15: 132–135.
22. Matsushima F, Meshitsuka S. Ingestion and excretion of aluminum in foods and pharmaceuticals. Nippon Eiseigaku Zasshi 2001; 56: 528–534. (in Japanese)

Molecular Psychiatry (2004) 9, 299–307

www.nature.com/mp

ORIGINAL RESEARCH ARTICLE

Expression analysis of neuregulin-1 in the dorsolateral prefrontal cortex in schizophrenia

R Hashimoto[1], RE Straub[1], CS Weickert[1], TM Hyde[1], JE Kleinman[1] and DR Weinberger*,[1]

[1]*Clinical Brain Disorders Branch, National Institute of Mental Health, Bethesda, MD, USA*

Genetic linkage and association have implicated neuregulin-1 (NRG-1) as a schizophrenia susceptibility gene. We measured mRNA expression levels of the three major isoforms of NRG-1 (ie type I, type II, and type III) in the postmortem dorsolateral prefrontal cortex (DLPFC) from matched patients and controls using real-time quantitative RT-PCR. Expression levels of three internal controls—GAPDH, cyclophilin, and β-actin—were unchanged in schizophrenia, and there were no changes in the absolute levels of the NRG-1 isoforms. However, type I expression normalized by GAPDH levels was significantly increased in schizophrenia DLPFC (by 23%) and positively correlated with antipsychotic medication dosage. Type II/type I and type II/type III ratios were significantly decreased (18 and 23% respectively). There was no effect on the NRG-1 mRNA levels of genotype at two SNPs previously associated with schizophrenia, suggesting that these alleles are not functionally responsible for abnormal NRG-1 expression patterns in patients. Subtle abnormalities in the expression patterns of NRG-1 mRNA isoforms in DLPFC may be associated with schizophrenia.
Molecular Psychiatry (2004) 9, 299–307. doi:10.1038/sj.mp.4001434
Published online 21 October 2003

Keywords: neuregulin-1; schizophrenia; expression; postmortem brain; isoform; dorsolateral prefrontal cortex

Introduction

Schizophrenia is a complex genetic disorder affecting 0.5–1% of the general population worldwide. Several genome-wide linkage scan studies and meta-analysis of whole-genome linkage scans show a suggestive linkage to schizophrenia on chromosome 8p.[1–10] Recently, neuregulin-1 (NRG-1), which maps to the 8p locus, has been implicated as a susceptibility gene for schizophrenia by a combination of linkage and association analyses.[11,12] NRG-1 is one of the neuregulin family of proteins, which have a broad range of bioactivities in the central nervous system and contain an epidermal growth factor (EGF)-like motif that activates membrane-associated tyrosine kinases related to ErbB receptors.[13] The EGF-like domain of NRG-1 is required for ErbB receptor binding, dimerization, tyrosine phosphorylation, and activation of downstream signaling pathways.[14] A gene-targeting approach for NRG-1-ErbB signaling revealed a behavioral phenotype in mice that overlaps with certain animal models for schizophrenia. For example, NRG-1 and ErbB4 mutant mice exhibit elevated activity levels in an open field, which was reversed by clozapine, and abnormal sensorimotor gating measured by prepulse inhibition of the startle reflex.[11,15]

The NRG-1 gene generates multiple alternative splicing variants, classified into three primary isoform groups.[16] NRG-1 type I (heregulin/ARIA: acetylcholine receptor-inducing activity/NDF: neu differentiation factor) has an immunogloblin-like domain, followed by a region of high glycosylation; type II (GGF: glial growth factor) has GGF-specific and immunogloblin-like domains; and type III (SMDF: sensory and motor neuron-derived factor) has a cysteine-rich domain. These NRG-1 isoforms play multiple and distinct functions in neuronal development, and abnormalities in brain development have been implicated in schizophrenia. Moreover, NRG-1 regulates the expression and plasticity of *N*-methyl-*d*-aspartate receptors (NMDAR), of the β2 subunit of the γ-amino butyric acid receptor, and of nicotinic acetylcholine receptor subtypes including α5, α7, and β4 subunits[17–20], some of which also may be involved in genetic risk for schizophrenia.[21,22]

Thus, while genetic evidence implicates NRG-1 as a schizophrenia susceptibility gene, and the biology of NRG-1 overlaps with diverse aspects of the putative biology of schizophrenia, there have been no published studies of NRG-1 expression in the schizophrenic brain tissue, and little is known about whether a specific NRG-1 isoform contributes to the risk for schizophrenia. Here, we employed a real-time quantitative RT-PCR technique to explore the mRNA

*Correspondence: Dr DR Weinberger, MD Chief, Clinical Brain Disorders Branch, IRP, National Institute of Mental Health, NIH, Room 4S-235, 10 Center Drive, Bethesda, MD 20892, USA.
E-mail: weinberd@intra.nimh.nih.gov
Received 21 April 2003; revised 25 August 2003; accepted 10 September 2003

expression of each type of NRG-1 in the dorsolateral prefrontal cortex (DLPFC), where prominent functional and neuroanatomical abnormalities have often been observed in schizophrenia.[23]

Materials and methods

Human postmortem tissue and RNA extraction
Postmortem DLPFC tissues from brains were collected at the Clinical Brain Disorders Branch, as previously described. [24] Diagnoses were retrospectively established by two psychiatrists using DSM-IV criteria. We endeavored within practical limits to derive a rough approximation of lifetime neuroleptic exposure, recognizing that this is an uncertain estimate. All available records, including inpatient and outpatient clinic records, were meticulously reviewed for every subject. Each reference, anywhere in the chart, to a new medication and to a change in dose of an old medication was catalogued. While it was impossible to exclude potential discontinuities in treatment (or patient noncompliance), in general, contiguous dose information was available for almost every subject. The total daily dose of neuroleptic medication given to the patients was calculated by adding the various daily medication levels and converting these levels to chlorpromazine (CPZ) equivalents, as previously formulated.[25] A median value of drug dosage was then derived from the CPZ equivalents to give the estimated average daily dose; this value was multiplied by the duration of illness (estimated from the earliest age of definable symptoms or age at first hospitalization) to give the estimated lifetime CPZ equivalents. Samples were matched for age, gender, ethnicity, brain pH, hemisphere, postmortem interval (PMI), and months in freezer (MIF). Demographic data are shown in Table 1.

The tissue blocks were dissected from the middle, superior, or inferior frontal gyrus from a 1–1.5 cm coronal slab just anterior to the corpus collosum. The blocks contained primarily gray matter and a small, but presumably random, amount of white matter. In order to test for the possibility of systematic difference in the gray matter/white matter ratio in the dissections of PFC from patients and controls, the total RNA extracted from these blocks was screened by microarray expression profiling for the content of mRNAs highly expressed in white matter such as glial fibrillary acidic protein (GFAP) and myelin basic protein (MBP). No significant differences in GFAP mRNA levels or MBP mRNA levels in RNA from patients with schizophrenia compared to controls were found (M Vawter, personal communication). While this approach does not conclusively rule out a systematic difference in the ratio of gray to white matter compartments in the tissue sampled from the schizophrenic and control groups, it reduces the likelihood of such an artifact.

The tissues were pulverized and stored at −80°C until use. Total RNA was extracted from 300–500 mg of DLPFC using TRIZOL Reagent (Life Technologies Inc., Grand Island, NY, USA), as previously described.[26] The yield of total RNA was determined by absorbance at 260 nm and the quality of total RNA was also analyzed using agarose gel electrophoresis.

DNAse treatment and reverse transcriptase reaction
Total RNA was treated with DNase for the removal of contaminating genomic DNA using DNase Treatment & Removal Reagents (Ambion, Austin, TX, USA), according to the manufacturer's protocol. After DNase treatment, the quality of total RNA was examined using agarose gel electrophoresis. Total RNA (6.8 μg) treated with DNase was used in 50 μl of reverse transcriptase reaction to synthesize cDNA, by using a SuperScript first-strand synthesis system for RT-PCR (Invitrogen, Carlsbad, CA, USA), according to the manufacturer's protocol. Briefly, total RNA (6.8 μg) was denatured with 1 mM of dNTP and 5 ng/μl of random hexamers at 65°C for 5 min. After the addition of RT buffer, $MgCl_2$ (5 mM in final concentration), dithiothreitol (10 mM in final concentration), RNAseOUT recombinant ribonuclease inhibitor (100 U), and SuperScriptII RT (125 U), the reaction mixture was incubated at 25°C for 10 min, at 42°C for 40 min, and at 70°C for 15 min. RNAse H (5 U) was added to the reaction mixture and then incubated at 37°C for 20 min.

Real-time quantitative PCR
The structure of human NRG-1 transcripts annotated in NCBI databases and the locations of each PCR amplicon are shown in Figure 1. We designed specific primer and probe combinations to recognize each NRG-1 isoform family as follows: type I: exons 4 and 5, type II: exons 4 and 8, and type III: exons 7 and 8.

NRG-1 mRNA expression levels were measured by real-time quantitative RT-PCR, using each combination of oligonucleotides and an ABI Prism 7900 sequence detection system with 384-well format (Applied Biosystems, Foster City, CA, USA). Each 20 μl PCR reaction contained 6 μl of cDNA, 900 nM of each primer, 250 nM of probe, and 10 μl of TaqMan Universal PCR Mastermix (Applied Biosystems) containing AmpliTaq Gold DNA polymerase, AmpErase UNG, dNTPs with dUTP, passive reference, and optimized buffer components. The PCR cycling conditions were 50°C for 2 min, 95°C for 10 min, 40 cycles of 95°C for 15 s, and 59°C or 60°C for 1 min. PCR data were obtained with the Sequence Detector Software (SDS version 2.0, Applied Biosystems) and quantified by a standard curve method. This software plotted the real-time fluorescence intensity and selected the threshold within the linear phase of the amplicon profile. The software plotted a standard curve of the cycle at threshold (Ct) (where the fluorescence generated within a reaction and threshold crosses) *vs* quantity of RNA. All samples were measured in one plate for one target gene or isoform, and their Ct values were in the linear range of the standard curve. Experiments were typically performed three times with triplicate determination and each gene expression level was determined by the

Table 1 Demography in the formation of the Clinical Brain Disorder Branch cohort

Case number	*Diagnosis*	*Age*	*Sex*	*Race*	*Side*	*pH*	*PMI (h)*	*Month in freezer*	*Cause of death*	*Manner of death*	*Age of onset/ duration of illness (year)*	*Last CPZ (eq/mg)*	*Daily CPZ (eq/mg)*	*Lifetime CPZ (eq/kg)*
1	CON	68	M	AA	L	6.57	22.5	192	ASCVD	natural				
2	CON	58	F	AA	L	6.54	26.5	226	ASCVD	natural				
3	CON	39	F	AA	L	6.34	40.5	226	Cardiac arrest	natural				
4	CON	46	F	AA	L	5.93	19.5	147	Dilated cardiomyopathy	natural				
5	CON	45	M	C	L	6.61	16.0	144	Blunt force injuries	accident				
6	CON	47	M	AA	L	6.03	60.0	157	Acute bronchial asthma	N/A				
7	CON	77	M	AA	R	6.06	18.5	146	Occlusive coronary atherosclerosis	natural				
8	CON	55	M	AA	R	6.00	9.5	146	MI (ASCVD)	natural				
9	CON	60	F	C	L	6.40	8.0	145	ASCVD	natural				
10	CON	61	F	AA	R	6.15	61.0	145	Multiple blunt force injuries	accident				
11	CON	26	M	C	L	6.08	13.0	115	ASCVD	natural				
12	CON	52	F	AA	R	6.87	10.0	100	Ruptured aorta	natural				
13	CON	42	M	AA	R	6.63	40.0	97	Acute asthma attack	natural				
14	CON	24	M	AA	R	6.59	12.5	96	Fibrinous pericarditis	natural				
15	CON	38	M	AA	R	6.14	32.5	95	Pulmonary embolism	accident				
16	CON	56	M	AA	R	6.09	33.0	88	Pulmonary embolism	natural				
17	CON	57	F	AA	R	6.43	19.0	76	MI-ASCVD	natural				
18	CON	59	F	AA	R	6.57	37.0	72	Cirrhosis of the liver	natural				
19	CON	67	F	AA	L	6.69	34.0	67	Cardiomyopathy Pulmonary edema	natural				
Mean (SD)		51.4 (13.8)				6.35 (0.28)	27.0 (15.8)	130.5 (47.8)						
20	SCH/TD	71	F	C	L	6.41	47.5	181	ASCVD	natural	15/56	100	500	0.6
21	SCH	36	M	AA	R	6.56	13.0	192	Blunt force injuries	suicide	21/16	400	850	5
22	SCH	46	M	AA	R	6.35	24.5	192	ASCVD	natural	23/23	N/A	N/A	N/A
23	SCH	44	F	AA	R	6.51	32.5	191	Cardiomegaly and hypertension	natural	19/15	200	200	1.1
24	SCH	46	M	AA	R	6.73	25.0	196	Blunt force injuries	suicide	36/10	300	300	1.1
25	SCH	48	M	C	R	6.29	13.5	146	Delusional hyponatremia and hypo-osmolar coma	undetermined	33/15	300	300	1.6
26	SCH	73	M	C	R	6.00	13.5	143	ASCVD	natural	23/50	450	450	4.6
27	SCH	34	M	AA	R	6.23	34.5	141	Acute benzotropine intoxication	undetermined	26/8	N/A	N/A	N/A
28	SCH	75	M	AA	L	6.29	41.5	121	Undetermined	natural	29/46	400	400	5.3
29	SCH	64	F	AA	R	6.48	19.5	121	Asphyxia due to aspiration	accident	19/45	900	400	5.3
30	SCH	67	F	AA	R	6.63	38.5	118	Chronic obstructive pulmonary disease	natural	30/37	80	100	1.3
31	SCH	31	M	C	R	6.46	14.0	112	Cerebral edema	natural	17/14	200	N/A	N/A
32	SCH	23	M	AA	L	6.48	42.5	112	Respiratory arrest	natural	21/2	400	480	0.033
33	SCH	60	F	AA	L	6.38	19.0	110	ASCVD	natural	40/20	100	100	0.7
34	SCH	30	M	AA	L	6.32	72.5	106	Pneumonia	natural	18/12	1900	500	2.2
35	SCH	81	F	C	R	6.78	11.0	100	ASCVD	natural	27/54	100	150	2.1

Table 1 Continued

Case number	Diagnosis	Age	Sex	Race	Side	pH	PMI (h)	Month in freezer	Cause of death	Manner of death	Age of onset/ duration of illness (year)	Last CPZ (eq/mg)	Daily CPZ (eq/mg)	Lifetime CPZ (eq/kg)
36	SCH/TD	61	F	AA	R	6.74	20.0	95	Asphyxiation	accident	24/27	N/A	200	2
37	SCH/TD	38	M	AA	R	6.50	61.0	89	Acute peritonities	accident	16/27	800	60	11.8
38	SCH	41	F	AA	R	6.08	51.0	80	ASCVD	natural	16/25	2400	1135	10.4
39	SCH/TD	41	M	AA	L	6.63	32.0	76	ASCVD	natural	20/21	50	400	2.5
Mean		50.5				6.44	31.3	131.1			23.7/26.2	534	343	3.03
(SD)		(17.1)				(2.21)	(17.3)	(39.8)			(7.0/16.3)	(659)	(287)	(3.35)

Means and standard deviations are printed below the last individual in each group. CON=normal control; SCH=schizophrenia; TD=tardive dyskinesia; M=male; F=female; AA=African American; C=Caucasian; R=right; L=left; PMI=post-mortem interval; N/A=not available; CPZ=chlorpromazine; eq=equivalent.

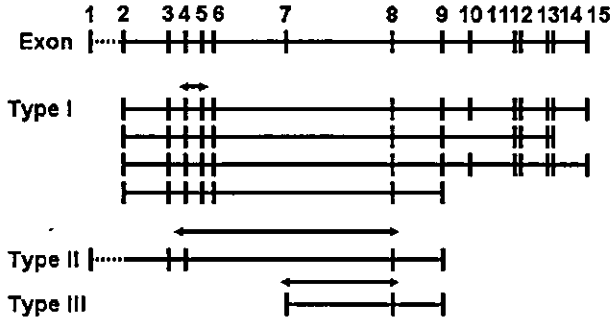

Figure 1 NRG-1 structure and probe design. Human NRG-1 mRNA has 15 exons. The exon usages of type I, type II or type III isoforms of NRG-1 are shown. Arrows indicate the location of primers and probes specific for type I, type II or type III isoforms of NRG-1.

average of three independent experiments. Predicted Ct values and sample quantities were used for statistical analysis.

Oligonucleotide primers and standard curve construction

Primer and probe sequences were designed by using PRIMER EXPRESS software (version 2.0, Applied Biosystems). Agarose gel electrophoresis was used to verify the size predictions of PCR amplicons (data not shown). The TaqMan Pre-Developed Assay Reagent kit (Applied Biosystems) was used for housekeeping genes: GAPDH, β-actin, and cyclophilin. The real-time PCR (TaqMan) detection of NRG-1 isoforms used the following oligonucleotides: type I, forward primer P3089 5′-GCCAATATCACCATCGTGGAA-3′, reverse primer P3090 5′-CCTTCAGTTGAGGCTGGCATA-3′, probe P3091 5′-FAM-CAAACGAGATCATCACTG-MGB-3′; type II, forward primer P3092 5′-GAATCA-AACGCTACATCTACATCCA-3′, reverse primer P3093 5′-CCTTCTCCGCACATTTTACAAGA-3′, probe P3094 5′-FAM-CACTGGGACAAGCC-MGB-3′; type III, forward primer P3095 5′-CAGCCACAAACAACAGAA-ACTAATC-3′, reverse primer P3096 5′-CCCAGTG-GTGGATGTAGATGTAGA-3′, probe P3097 5′-FAM-CCAAACTGCTCCTAAAC-MGB-3′(purchased from Applied Biosystems). These primers were designed to amplify specific transcripts based on the unique exon structure of each isoform. Thus, for example, because isoform II lacks exons 5–7, primers focused on exons 4 and 8, which are contiguous in the isoform II transcript, and will amplify only this isoform. Standard curves for the housekeeping genes and the three NRG-1 isoforms were prepared using serial dilutions (1:4) of pooled cDNA from total RNA derived from DLPFC of six normal control subjects (Figure 2). In each experiment, the R^2 value of the standard curve was more than 0.99 and no-template control assays resulted in no detectable signal.

SNP genotyping

DNA was extracted from brain tissue using standard methods. P3149SNP8NRG221533 and SNP8NRG24-

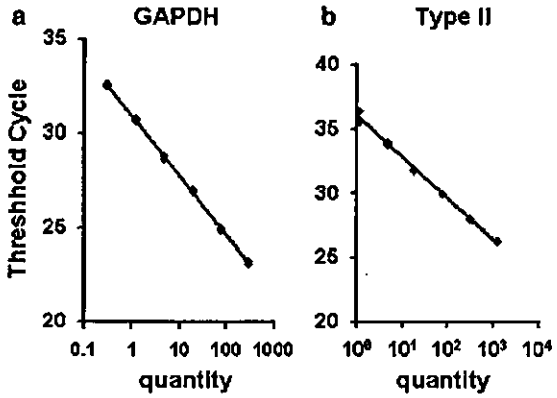

Figure 2 Standard curves for control (housekeeping genes) and NRG-1 type II. Standard curves for GAPDH (a) and type II (b). The quantity represents an amount of cDNA prepared from 1 ng of total RNA in the PCR reaction. R^2 values are 1.000 and 0.995 for GAPDH and type II.

3177P3155 genotypes were determined using the Taqman 5′-exonuclease allelic discrimination assay. These SNPs were chosen because they showed the strongest association to schizophrenia in prior studies.[11,12] Probes and primers for detection of the SNP are: SNP8NRG221533, forward primer P3151 5′-AAGGCATCAGTTTTCAATAGCTTTTT-3′, reverse primer P3152 5′-TAAGTAGAAATGGGAACTCTCCATCTC-3′, probe1 P3149 5′-FAM-TTTATTTTgCCAAATAT-MGB-3′, probe2 P3150 5′-VIC-TCTTTATTTTaCCAAATATCAT-MGB-3′; SNP8NRG243177, forward primer P3159 5′-AATTAGTAGGATTGGATGTTTGAACCA-3′, reverse primer P3160 5′-GATGGAGCGCTTCAGGAGAA-3′, probe1 P3155 5′-FAM-CCAGTATACgTTCACTTG-MGB-3′, probe2 P3156 5′-VIC-CCAGTATACaTTCAC-TTGA-MGB-3′. Each 10 μl PCR reaction contained 10 ng of DNA, 1 μM of each primer, 100 nM of each probe, and 5 μl of TaqMan Universal PCR Mastermix (Applied Biosystems) containing AmpliTaq Gold DNA polymerase, AmpErase UNG, dNTPs with dUTP, passive reference, and optimized buffer components. The PCR cycling conditions were at 50°C for 2 min, 95°C for 10 min, 40 cycles of 95°C for 15 s, and 60°C for 1 min.

Statistical analysis

An independent *t*-test was used to compare the age, brain pH, months in freezer, and postmortem interval, and a Mann–Whitney *U*-test was used to compare the gene expression levels between schizophrenic and control groups with Statistica software (release 5.5, Statsoft, Inc., Tulsa, OK, USA). The groups did not differ in gender and ethnicity. Differences in NRG-1 expression levels between groups were also analyzed by ANCOVA, with diagnosis as the independent factor and brain pH and age as covariates. Spearman rank order correlation test was used for comparison between demographic data and expression data.

Results

Control genes and NRG-1 mRNA levels

The expression levels of three standard 'housekeeping' genes—GAPDH, β-actin, and cyclophilin—were not significantly different between groups (Figure 3a). Raw (ie nonnormalized) NRG-1 isoform expression levels also did not differ between groups (Figure 3b).

Effects of demographics on NRG-1 mRNA expression levels

Expression levels of all the three NRG-1 isoforms normalized by cyclophilin were positively correlated with age in normal control subjects (Rho=0.637, P=0.006; Rho=0.573, P=0.015, and Rho=0.637, P=0.013 for type I, type II, and type III, respectively); however, there was no correlation between normalized NRG-1 isoform expression levels and age in schizophrenia patients (all $P>0.6$). Similar results were obtained with normalization to GAPDH and β-actin (data not shown). NRG-1 expression levels were not associated with sex, race or hemisphere, and did not correlate with PMI or MIF. Brain pH and type I mRNA expression normalized by cyclophilin were correlated in both normal control (Rho=−0.477, P=0.050) and schizophrenia groups (Rho=−0.500,

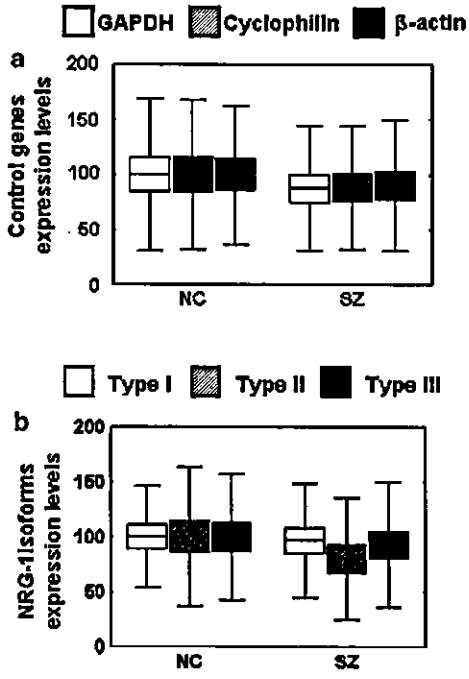

Figure 3 mRNA expression levels of NRG-1 isoforms. The expression levels of housekeeping genes (a) and NRG-1 isoforms (b) were measured in the DLPFC of normal control subjects (NC) and patients with schizophrenia (SZ). The expression levels were calculated by comparison to the percentage of average of normal control subjects. Boxes and bars outside boxes represent the standard error and standard deviation. Bars in boxes represent means.

P=0.041), with similar results normalizing by GAPDH or β-actin. Thus, brain pH (as well as age) was used as covariate for type I expression data analysis.

Normalized NRG-1 mRNA levels

NRG-1 type I expression levels normalized by GAPDH, cyclophilin or β-actin (to reduce the effects of possible mRNA degradation not detectable by electrophoresis and/or possible variations in RT efficiency) were increased by 23, 18 or 16%, respectively, in schizophrenia patients (ANCOVA: all $P<0.050$). (Figure 4a). No significant differences were observed between groups in normalized NRG-1 type II and type III expression levels (Figure 4b, c).

We further analyzed the expression ratios among the three types of NRG-1 isoforms to investigate possible isoform–isoform interactions or altered regulation of splicing (Figure 5). There was no significant difference in type I/type III expression ratio with or without covariates (age and pH) (normal control: 100.0 (mean) ±33.8 (SD) *vs* schizophrenia patients: 109.1±36.8). However, both type II/type III and type II/type I expression ratios were significantly decreased in the schizophrenic group (17 and 23%, Mann–Whitney U-test: P=0.010 and 0.013, respectively). ANCOVA with brain pH and age as covariates did not alter the statistical significance of this relative type II decrease (type II/type I; F=10.96, P=0.002, df=1, 32).

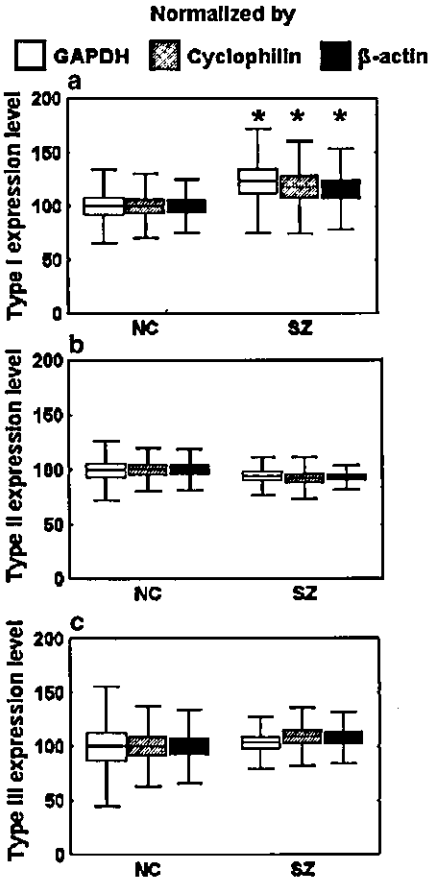

Figure 4 Relative expression levels of NRG-1 type I (a), type II (b), and type III (c) isoforms normalized by GAPDH, cyclophilin or β-actin in the DLPFC of normal control subjects (NC) and patients with schizophrenia (SZ). Significant group differences by ANCOVA are indicated by *$P<0.05$.

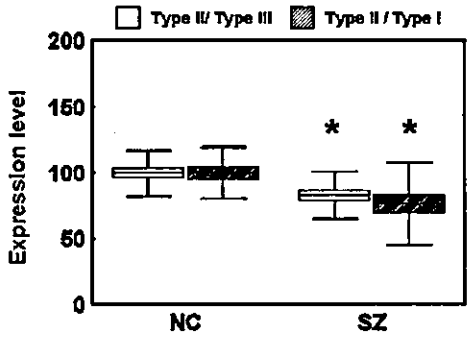

Figure 5 Relative expression ratios of Type II normalized by Type I or Type III in DLPFC of normal control subjects (NC) and patients with schizophrenia (SZ). *$P < 0.05$.

Influence of clinical characteristics on NRG-1 expression

None of the measurements of NRG-1 isoforms correlated significantly with the age of onset, duration of illness or last and lifetime dose of chlorpromazine equivalents (data not shown). A positive correlation between type I expression levels normalized by cyclophilin and daily dose was found (Rho=0.601, P=0.014), although daily dose was not correlated with normalized type II or type III expression levels (Rho=−0.315, P=0.218; Rho=−0.102, P=0.681, respectively). Similar results were obtained after normalization by GAPDH and β-actin (data not shown).

Allele effects on NRG-1 expression

No effect of SNP8NRG221533 genotype, which has been reported to be associated with schizophrenia in both Icelandic and Scottish populations,[11,12] was apparent in type I, type II, and type III expression levels normalized by cyclophilin, and the expression ratio of type II/type III in total subjects, normal controls or patients. For example, one allele homozygote (N=21) had mean levels of type I expression of 100.9±37.6 (SD), while two carriers (N=12) had 99.2±28.3 (SD) ($P>0.8$). Neither NRG-1 expression levels normalized by GAPDH or β-actin nor the other combinations of isoform–isoform expression ratio were affected by this genotype in any group (data not shown). Similar negative results were obtained between NRG-1 expression and SNP8NRG243177 (data not shown), which also has been associated with schizophrenia.[11,12]

Discussion

In this study, we have measured mRNA expression levels of NRG-1 isoforms in DLPFC using real-time quantitative RT-PCR in patients with schizophrenia and in normal controls. NRG-1 has been implicated as a susceptibility gene in schizophrenia. We found preliminary evidence that the pattern of expression of NRG-1 isoforms may be abnormal in schizophrenia. Specifically, there was a small increase in type I expression levels, and a small decrease of type II/type I and type II/type III ratios in the patients with schizophrenia. As consistent results were obtained from normalization of NRG-1 isoforms by all the three housekeeping genes, our findings would seem to be robust at least in comparison to results that might have been based on using only one control gene. Our data appear to add to the evidence that NRG-1 may be involved in schizophrenia, but other explanations, for example, differences in postmortem stability of the various isoforms, cannot be excluded. Moreover, as our study did not include measurement of the levels of NRG-1 proteins, of expression in other brain regions or in other psychiatric disorders, further work is necessary to clarify whether changes in NRG-1 mRNA impact on protein expression and is regionally and diagnostically specific..

NRG-1 binds to its receptor, ErbB, and NRG-1-ErbB signaling plays multiple roles in development and plasticity in the central nervous system.[13] Type I is prominently expressed early in development; type II is abundantly expressed in the adult nervous system; and type III is the major isoform produced by sensory neurons and motorneurons, and is also expressed in the rodent brain.[27] Little is known about NRG-1 expression in human brain; however, NRG-1 is present in neuronal cell bodies and synapse-rich regions in the hippocampus and type II isoform is expressed in oligodendrocytes, astrocytes, and microglia.[28,29] We detected mRNA of each of the three major classes of NRG-1 isoforms in human DLPFC, but we did not characterize the multiple spice variants within these isoforms. We also found a positive correlation between expression levels of each of the NRG-1 isoforms with age in normal subjects, suggesting that NRG-1 mRNA increases as the prefrontal cortex ages. However, the meaning of this correlation is unclear, and it was not found in the patients.

NRG-1 type I has been implicated in neuronal plasticity because it shows activity-dependent regulation, and it is involved in regulating neurotransmitter receptor expression. Multiple perturbations in neuronal activity have been shown to affect type I expression. For example, seizures, long-term potentiation, and forced locomotion induce type I expression in the hippocampus, amygdala, and motor cortex. Brain injury induces NRG-1 protein expression in astrocytes of rat cerebral cortex.[30] Curare blockade of nicotinic receptors reduces the expression of type 1 protein in chick motor neurons, an effect that can be prevented by brain-derived neurotrophic factor and neurotrophin 3.[31] In the central nervous system, NRG-1 promotes the switch from the immature form of NMDAR, which contains primarily NR2B subunits to one containing more NR2C subunits.[17] NRG-1 also potentiates $\alpha 7$ nicotinic acetylcholine receptor transmission in hippocampal neurons,[20] and expression of the $\beta 2$ subunit of the γ-amino butyric acid receptor in cerebellar granule cells.[19] Thus, the relative increase in type I expression in schizophrenia brain might alter neuronal signaling of NRG-1 *per se*, or it may be an indirect factor in putative abnormalities of NMDA, nicotinic, and/or GABA receptor-related signaling in schizophrenia brain.[21,32,33] The positive correlation between type I expression level and the daily dose of chlorpromazine equivalents suggests that this upregulation of type I could reflect a relationship between NRG-1 expression level and illness severity. Alternatively, it might be due to neuroleptic treatment. We are currently exploring in animals the potential effect of antipsychotic medication on NRG-1 expression.

NRG-1 type II (GGF) is also of central importance for neuronal and glial development. Type II is expressed in developing cortical neurons, and it promotes the transformation and differentiation of radial glial cells, which in turn support cortical neuronal cell migration and differentiation.[34] A study using NRG-1-deficient mice revealed that NRG-1-erbB2 signaling is required for the establishment of radial glia and their transformation into astrocytes in cerebral cortex.[35] In our study, decreased ratios of type II/type I and type II/type III may be due to relative underexpression of type II in DLPFC of schizophrenia patients. Neuroanatomical abnormalities have been reported in DLPFC in schizophrenia, including abnormal neuropil and cytoarchitecture.[36–40] It is unclear whether variations in NRG-1 expression could relate to these changes. In addition, a change in the balance of type I/type II to type III NRG-1 may influence cholinergic neurotransmission, as the distinct isoforms differentially induce various subunits of the nAChR.[18]

Although NRG-1 was first recognized to be critical for multiple stages of schwann cell development[41,42], its role in promoting the development of myelin-forming cells is now recognized to include oligodendrocytes. Not only is NRG-1 and various ErbB receptors expressed in the subependymal zone and the forebrain oligogenic zone, but NRG-1 can also induce the division[43] and/or promote the differentiation of oligodendrocyte precursors *in vitro*.[44–47] It is conceivable that relatively decreased type II mRNA expression may relate to putative abnormalities of oligodendroglial function implicated in schizophrenia.[48,49] Finally, we did not find evidence that NRG-1 type III mRNA expression levels are changed in schizophrenia DLPFC, although this isoform also has effects on neuronal plasticity and development.[18,50]

The multiple marker haplotype in the NRG-1 gene that has been associated with schizophrenia spans the

first exon, which is the promoter region for type II and is far upstream from the exons of all other isoforms.[11,12] The functional allele contributing to the increased risk for schizophrenia has not been identified in NRG-1, nor is there evidence that any of the associated variations would impact gene expression or function. As two single SNPs associated with schizophrenia were located around the promoter region of NRG-1 and the first exon of GGF, these SNPs might regulate the expression levels of NRG-1 isoforms and/or isoform–isoform ratios. However, no obvious allele effects of these SNPs on NRG-1 expression patterns were observed in this small sample. The estimated relative risks of each of these markers alone were less than that of the seven-marker core haplotype.[11,12] Taken together, these two SNPs do not appear to be functional alleles, at least in terms of the regulation of NRG-1 expression in human DLPFC. However, the possible relative decrease in type II expression may be regulated by an as yet unidentified allele in linkage disequilibrium with the associated haplotype.

Our findings offer preliminary evidence that abnormal expression of NRG-1 isoforms in DLPFC may be related to the pathophysiology of schizophrenia, but the evidence is weak. The biologic implications of our results are unknown, but they are at least conceptually consistent with evidence that schizophrenia involves genetic abnormalities in developmental/plasticity-related processes.[51,52] Additional studies are needed to characterize NRG-1 expression in schizophrenia, including slide-based mRNA analyses, protein analyses, neuroleptics effects, diagnostic specificity, and further exploration of genotype based variation.

Acknowledgements

We wish to thank Drs Takashi Morihara, Toyoko Hiroi, and Masasumi Kamohara for advice on real-time quantitative PCR. We also thank Dr Kenichiro Miura for advice of statistical analysis and Dr Vakkalanka Radhakrishna and Dr Bhaskar Kolachana for SNP genotyping and Dr Gerry Fischbach for review of the manuscript. This work was supported in part by the Essel Foundation through a NARSAD distinguished investigator award to DRW.

References

1 Pulver AE, Lasseter VK, Kasch L, Wolyniec P, Nestadt G, Blouin JL *et al.* Schizophrenia: a genome scan targets chromosomes 3p and 8p as potential sites of susceptibility genes. *Am J Med Genet* 1995; **60**: 252–260.
2 Kendler KS, MacLean CJ, O'Neill FA, Burke J, Murphy B, Duke F *et al.* Evidence for a schizophrenia vulnerability locus on chromosome 8p in the Irish Study of high-density schizophrenia families. *Am J Psychiatry* 1996; **153**: 1534–1540.
3 Blouin JL, Dombroski BA, Nath SK, Lasseter VK, Wolyniec PS, Nestadt G *et al.* Schizophrenia susceptibility loci on chromosomes 13q32 and 8p21. *Nat Genet* 1998; **20**: 70–73.
4 Kaufmann CA, Suarez B, Malaspina D, Pepple J, Svrakic D, Markel PD *et al.* NIMH Genetics Initiative Millenium Schizophrenia Consortium: linkage analysis of African-American pedigrees. *Am J Med Genet* 1998; **81**: 282–289.
5 Shaw SH, Kelly M, Smith AB, Shields G, Hopkins PJ, Loftus J *et al.* A genome-wide search for schizophrenia susceptibility genes. *Am J Med Genet* 1998; **81**: 364–376.
6 Brzustowicz LM, Honer WG, Chow EW, Little D, Hogan J, Hodgkinson K *et al.* Linkage of familial schizophrenia to chromosome 13q32. *Am J Hum Genet* 1999; **65**: 1096–1103.
7 Gurling HM, Kalsi G, Brynjolfson J, Sigmundsson T, Sherrington R, Mankoo BS *et al* . Genomewide genetic linkage analysis confirms the presence of susceptibility loci for schizophrenia, on chromosomes 1q322, 5q33.2, and 8p21–22 and provides support for linkage to schizophrenia, on chromosomes 11q23.3–24 and 20q12.1–11.23. *Am J Hum Genet* 2001; **68**: 661–673.
8 Badner JA, Gershon ES. Meta-analysis of whole-genome linkage scans of bipolar disorder and schizophrenia. *Mol Psychiatry* 2002; **7**: 405–411.
9 DeLisi LE, Mesen A, Rodriguez C, Bertheau A, LaPrade B, Llach M *et al.* Genome-wide scan for linkage to schizophrenia in a Spanish-origin cohort from Costa Rica. *Am J Med Genet* 2002; **114**: 497–508.
10 Straub RE, MacLean CJ, Ma Y, Webb BT, Myakishev MV, Harris-Kerr C *et al.* Genome-wide scans of three independent sets of 90 Irish multiplex schizophrenia families and follow-up of selected regions in all families provides evidence for multiple susceptibility genes. *Mol Psychiatry* 2002; **7**: 542–559.
11 Stefansson H, Sigurdsson E, Steinthorsdottir V, Bjornsdottir S, Sigmundsson T, Ghosh S *et al.* Neuregulin 1 and susceptibility to schizophrenia. *Am J Hum Genet* 2002; **71**: 877–892.
12 Stefansson H, Sarginson J, Kong A, Yates P, Steinthorsdottir V, Gudfinnsson E *et al.* Association of neuregulin 1 with schizophrenia confirmed in a Scottish population. *Am J Hum Genet* 2003; **72**: 83–87.
13 Fischbach GD, Rosen KM. ARIA: a neuromuscular junction neuregulin. *Annu Rev Neurosci* 1997; **20**: 429–458.
14 Murphy S, Krainock R, Tham M. Neuregulin signaling via erbB receptor assemblies in the nervous system. *Mol Neurobiol* 2002; **25**: 67–77.
15 Gerlai R, Pisacane P, Erickson S. Heregulin, but not ErbB2 or ErbB3, heterozygous mutant mice exhibit hyperactivity in multiple behavioral tasks. *Behav Brain Res* 2000; **109**: 219–227.
16 Buonanno A, Fischbach GD. Neuregulin and ErbB receptor signaling pathways in the nervous system. *Curr Opin Neurobiol* 2001; **11**: 287–296.
17 Ozaki M, Sasner M, Yano R, Lu HS, Buonanno A. Neuregulin-beta induces expression of an NMDA-receptor subunit. *Nature* 1997; **390**: 691–694.
18 Yang X, Kuo Y, Devay P, Yu C, Role L. A cysteine-rich isoform of neuregulin controls the level of expression of neuronal nicotinic receptor channels during synaptogenesis. *Neuron* 1998; **20**: 255–270.
19 Rieff HI, Raetzman LT, Sapp DW, Yeh HH, Siegel RE, Corfas G. Neuregulin induces GABA(A) receptor subunit expression and neurite outgrowth in cerebellar granule cells. *J Neurosci* 1999; **19**: 10757–10766.
20 Liu Y, Ford B, Mann MA, Fischbach GD. Neuregulins increase alpha7 nicotinic acetylcholine receptors and enhance excitatory synaptic transmission in GABAergic interneurons of the hippocampus. *J Neurosci* 2001; **21**: 5660–5669.
21 Freedman R, Leonard S, Gault JM, Hopkins J, Cloninger CR, Kaufmann CA *et al.* Linkage disequilibrium for schizophrenia at the chromosome 15q13–14 locus of the alpha7-nicotinic acetylcholine receptor subunit gene (CHRNA7). *Am J Med Genet* 2001; **105**: 20–22.
22 Leonard S, Gault J, Hopkins J, Logel J, Vianzon R, Short M *et al.* Association of promoter variants in the alpha7 nicotinic acetylcholine receptor subunit gene with an inhibitory deficit found in schizophrenia. *Arch Gen Psychiatry* 2002; **59**: 1085–1096.
23 Weinberger DR, Egan MF, Bertolino A, Callicott JH, Mattay VS, Lipska BK *et al.* Prefrontal neurons and the genetics of schizophrenia. *Biol Psychiatry* 2001; **50**: 825–844.
24 Kleinman JE, Hyde TM, Herman MM. Methodological issues in the neuropathology of mental illness. In: Bloom FE, Kupfer DJ (eds). *Psychopharmacology: The Fourth Generation of Progress.* Raven Press, Ltd: New York, 1999, pp 859–864.

25 Torrey EF. *Surviving schizophrenia.* Harper & Row: New York, 1983.
26 Weickert CS, Hyde TM, Lipska BK, Hearman MM, Weinberger DR, Kleinman JE. Reduced brain-derived neurotrophic factor in prefrontal cortex of patients with schizophrenia. *Mol Psychiatry* 2003; **8**: 592–610.
27 Garratt AN, Britsch S, Birchmeier C. Neuregulin, a factor with many functions in the life of a schwann cell. *BioEssays* 2000; **22**: 987–996.
28 Cannella B, Pitt D, Marchionni M, Raine CS. Neuregulin and erbB receptor expression in normal and diseased human white matter. *J Neuroimmunol* 1999; **100**: 233–242.
29 Chaudhury AR, Gerecke KM, Wyss JM, Morgan DG, Gordon MN, Carroll SL. Neuregulin-1 and erbB4 immunoreactivity is associated with neuritic plaques in Alzheimer disease brain and in a transgenic model of Alzheimer disease. *J Neuropathol Exp Neurol* 2003; **62**: 42–54.
30 Tokita Y, Keino H, Matsui F, Aono S, Ishiguro H, Higashiyama S *et al.* Regulation of neuregulin expression in the injured rat brain and cultured astrocytes. *J Neurosci* 2001; **21**: 1257–1264.
31 Loeb JA, Hmadcha A, Fischbach GD, Land SJ, Zakarian VL. Neuregulin expression at neuromuscular synapses is modulated by synaptic activity and neurotrophic factors. *J Neurosci* 2002; **22**: 2206–2214.
32 Benes FM, Berretta S. GABAergic interneurons: implications for understanding schizophrenia and bipolar disorder. *Neuropsychopharmacology* 2001; **25**: 1–27.
33 Tsai G, Coyle JT. Glutamatergic mechanisms in schizophrenia. *Annu Rev Pharmacol Toxicol* 2002; **42**: 165–179.
34 Anton ES, Marchionni MA, Lee KF, Rakic P. Role of GGF/neuregulin signaling in interactions between migrating neurons and radial glia in the developing cerebral cortex. *Development* 1997; **124**: 3501–3510.
35 Schmid RS, McGrath B, Berechid BE, Boyles B, Marchionni M, Sestan N *et al.* Neuregulin 1-erbB2 signaling is required for the establishment of radial glia and their transformation into astrocytes in cerebral cortex. *Proc Natl Acad Sci USA* 2003; **100**: 4251–4256.
36 Weickert CS, Kleinman JE. The neuroanatomy and neurochemistry of schizophrenia. *Psychiatr Clin North Am* 1998; **21**: 57–75.
37 Lewis DA, Cruz DA, Melchitzky DS, Pierri JN. Lamina-specific deficits in parvalbumin-immunoreactive varicosities in the prefrontal cortex of subjects with schizophrenia: evidence for fewer projections from the thalamus. *Am J Psychiatry* 2001; **158**: 1411–1422.
38 Pierri JN, Volk CL, Auh S, Sampson A, Lewis DA. Decreased somal size of deep layer 3 pyramidal neurons in the prefrontal cortex of subjects with schizophrenia. *Arch Gen Psychiatry* 2001; **58**: 466–473.
39 Rajkowska G, Halaris A, Selemon LD. Reductions in neuronal and glial density characterize the dorsolateral prefrontal cortex in bipolar disorder. *Biol Psychiatry* 2001; **49**: 741–752.
40 Selemon LD, Mrzljak J, Kleinman JE, Herman MM, Goldman-Rakic PS. Regional specificity in the neuropathologic substrates of schizophrenia: a morphometric analysis of Broca's area 44 and area 9. *Arch Gen Psychiatry* 2003; **60**: 69–77.
41 Meyer D, Birchmeier C. Multiple essential functions of neuregulin in development. *Nature* 1995; **378**: 386–390.
42 Riethmacher D, Sonnenberg-Riethmacher E, Brinkmann V, Yamaai T, Lewin GR, Birchmeier C. Severe neuropathies in mice with targeted mutations in the ErbB3 receptor. *Nature* 1997; **389**: 725–730.
43 Canoll PD, Musacchio JM, Hardy R, Reynolds R, Marchionni MA, Salzer JL. GGF/neuregulin is a neuronal signal that promotes the proliferation and survival and inhibits the differentiation of oligodendrocyte progenitors. *Neuron* 1996; **17**: 229–243.
44 Vartanian T, Corfas G, Li Y, Fischbach GD, Stefansson K. A role for the acetylcholine receptor-inducing protein ARIA in oligodendrocyte development. *Proc Natl Acad Sci USA* 1994; **91**: 11626–11630.
45 Raabe TD, Clive DR, Wen D, DeVries GH. Neonatal oligodendrocytes contain and secrete neuregulins *in vitro*. *J Neurochem* 1997; **69**: 1859–1863.
46 Raabe TD, Francis A, DeVries GH. Neuregulins in glial cells. *Neurochem Res* 1998; **23**: 311–318.
47 Calaora V, Rogister B, Bismuth K, Murray K, Brandt H, Leprince P *et al.* Neuregulin signaling regulates neural precursor growth and the generation of oligodendrocytes *in vitro*. *J Neurosci* 2001; **21**: 4740–4751.
48 Hof PR, Haroutunian V, Copland C, Davis KL, Buxbaum JD. Molecular and cellular evidence for an oligodendrocyte abnormality in schizophrenia. *Neurochem Res* 2002; **27**: 1193–1200.
49 Hakak Y, Walker JR, Li C, Wong WH, Davis KL, Buxbaum JD *et al.* Genome-wide expression analysis reveals dysregulation of myelination-related genes in chronic schizophrenia. *Proc Natl Acad Sci USA* 2001; **98**: 4746–4751.
50 Wolpowitz D, Mason TB, Dietrich P, Mendelsohn M, Talmage DA, Role LW. Cysteine-rich domain isoforms of the neuregulin-1 gene are required for maintenance of peripheral synapses. *Neuron* 2000; **25**: 79–91.
51 Weinberger DR. Cell biology of the hippocampal formation in schizophrenia. *Biol Psychiatry* 1999; **45**: 395–402.
52 Harrison PJ, Owen MJ. Genes for schizophrenia? Recent findings and their pathophysiological implications. *Lancet* 2003; **361**: 417–419.

THE JOURNAL OF BIOLOGICAL CHEMISTRY
Vol. 278, No. 26, Issue of June 27, pp. 23648–23655, 2003
Printed in U.S.A.

Specific Compositions of Amyloid-β Peptides as the Determinant of Toxic β-Aggregation*

Received for publication, December 16, 2002, and in revised form, April 23, 2003
Published, JBC Papers in Press, April 25, 2003, DOI 10.1074/jbc.M212785200

Yuji Yoshiike‡, De-Hua Chui‡, Takumi Akagi§, Nobuo Tanaka¶, and Akihiko Takashima‡‖

From the ‡Laboratory for Alzheimer's Disease and the §Laboratory for Neural Architecture, RIKEN Brain Science Institute, 2-1 Hirosawa, Wako-shi, Saitama, 351-0198, Japan and the ¶Department of Life Science, Tokyo Institute of Technology, 4259 Nagatsuda-cho, Yokohama-shi, Kanagawa, 226-8503, Japan

Alzheimer's disease (AD) may be caused by toxic aggregates formed from amyloid-β (Aβ) peptides. By using Thioflavin T, a dye that specifically binds to β-sheet structures, we found that highly toxic forms of Aβ-aggregates were formed at the initial stage of fibrillogenesis, which is consistent with recent reports on Aβ oligomers. Formation of such aggregates depends on factors that affect both nucleation and elongation. As reported previously, addition of Aβ42 systematically accelerated the nucleation of Aβ40, most likely because of the extra hydrophobic residues at the C terminus of Aβ42. At Aβ42-increased specific ratio (Aβ40: Aβ42 = 10: 1), on the other hand, not only accelerated nucleation but also induced elongation were observed, suggesting pathogenesis of early-onset AD. Because a larger proportion of Aβ40 than Aβ42 was still required for this phenomenon, we assumed that elongation does not depend only on hydrophobic interactions. Without any change in the C-terminal hydrophobic nature, elongation was effectively induced by mixing wild type Aβ40 with Italian variant Aβ40 (E22K) or Dutch variant (E22Q). We suggest that Aβ peptides in specific compositions that balance hydrophilic and hydrophobic interactions promote the formation of toxic β-aggregates. These results may introduce a new therapeutic approach through the disruption of this balance.

Fibrillar amyloid-β peptide (Aβ)[1] in β-sheet conformation is one of the main components of senile plaques, a pathological hallmark of Alzheimer's disease (AD) (1, 2). Aβ is cleaved from β-amyloid precursor protein (APP) by secretases whose enzymatic components are suggested to include presenilins and β-site APP cleaving enzyme (3, 4). Most mutations of both APP and presenilins are associated with early-onset familial Alzheimer's disease (5–10). Interestingly, such mutations are also associated with increased production of Aβ42, which is a longer isoform of various Aβ species (5–10). Aβ42 likely aggregates more rapidly than other Aβ peptides because it contains additional hydrophobic amino acids at its carboxyl terminus (11–13). The overexpression of structurally normal APP that results from an extra gene in trisomy 21 (Down's syndrome) almost invariably leads to the premature occurrence of classic AD neuropathology during middle adult years (14). Brains from younger Down's syndrome subjects often display "diffuse plaques" composed solely of Aβ42, whereas older Down's syndrome subjects display "cored plaques" composed of Aβ40, a shorter form, at the plaque center (15). Together, these findings provide strong evidence for the role of Aβ42 in AD and AD-like pathology. Here, we report the importance of Aβ compositions for promoting toxicity-associated β-aggregation.

EXPERIMENTAL PROCEDURES

Chemicals and Peptides—Thioflavin T (ThT) was obtained from Sigma. *N,N*-dimethylformamide, sodium lauryl sulfate (SDS), 28% ammonia solution, Tris (hydroxymethyl) aminomethane, and HEPES were purchased from Nacalai tesque (Kyoto, Japan). 1,1,1,3,3,3-hexafluoro-2-propanol (HFIP) was obtained from Wako Pure Chemical (Osaka, Japan). Glycerol was obtained from Junsei (Tokyo, Japan). Wild type β-amyloid1–40 of four lots (510818, 511024, 520311, 520130) and wild type Aβ1–42 of three lots (510523, 520116, 520323) were obtained from Peptide Institute (Osaka, Japan). Italian variant Aβ1–40 of a lot (P04010T1) was purchased from American Peptide Company (Sunnyvale, CA). Italian variant Aβ1–40, Dutch variant Aβ1–40, Italian variant Aβ1–42, and four other non-pathogenic variants Aβ1–40 (E22R, E22shortK, E22D and E22longE) were synthesized and purified at Research Resources Center of RIKEN Brain Science Institute. "shortK" is an amino acid residue that has a similar structure to Lys with only three methyl groups prior to the terminal amine. "longE" is a residue that has a similar structure to Glu with an additional methyl group, three in total. All peptide samples were high pressure liquid chromatography-purified to be more than 90% pure and were in trifluoroacetate salt form.

Aβ Sample Preparation—A stock solution of Aβ was prepared by dissolving powdered Aβ peptide in 100% HFIP to a final concentration of 1 mg/ml. After shaking for two hours at 4 °C, the Aβ stock solution was aliquoted into siliconized tubes and stored at −80 °C. Just prior to each experiment, aliquots were spin-vacuumed using an Integrated SpeedVac system (Savant). For experiments shown in figures except Fig. 1, aliquots of Aβ40 were redissolved in 50% HFIP/14% NH3 solution and then spin-vacuumed. They were then dissolved in a HEPES-buffered solution.

Fluorescence Spectroscopy (ThT Assay)—The degree of β-aggregation was determined using the fluorescent dye, ThT, which specifically binds to fibrous structures (16). First, Aβ stock solution (see above) was diluted with 5 or 10 mM HEPES-NaOH and 0.9% NaCl. ThT was added to each test sample to a final concentration of 10 μM. Each sample was prepared in 96-well Black Cliniplates (Labsystems) and shaken for 10 s prior to each measurement. Measurements were carried out every 20 min.

The relative degree of β-aggregation was assessed in terms of fluorescence intensity, which was measured at 37 °C using a Fluoroskan Ascent FL spectrophotometer (Labsystems, Finland). Measurements were performed at an excitation wavelength of 444 nm and an emission of 485 nm, wavelengths that result in the optimum detection of bound ThT. To account for background fluorescence, the fluorescence intensity measured from each control solution without Aβ was subtracted from that of each solution containing Aβ. By making three or six wells of each condition, their standard deviations were first calculated. They were then divided by the square root of n.

* The costs of publication of this article were defrayed in part by the payment of page charges. This article must therefore be hereby marked "*advertisement*" in accordance with 18 U.S.C. Section 1734 solely to indicate this fact.

‖ To whom correspondence should be addressed. Tel.: 81-48-467-9632; Fax: 81-48-467-5916; E-mail: kenneth@brain.riken.go.jp.

[1] The abbreviations used are: Aβ, amyloid-β peptide; AD, Alzheimer's disease; APP, β-amyloid precursor protein; ThT, Thioflavin T; HFIP, 1,1,1,3,3,3-hexafluoro-2-propanol; HEK, human embryonic kidney; MTT, 3-[4,5-dimethylthiazol-2-yl]-2,5-diphenyltetrazolium bromide.

Cell Cultures—Human embryonic kidney (HEK) 293 cells were used to test the toxic effects of Aβ-aggregation as assessed in the 3-[4,5-dimethylthiazol-2-yl]-2,5-diphenyltetrazolium bromide (MTT) assay (see below). They were grown in Dulbecco's modified Eagle's medium (Sigma) containing 10% fetal bovine serum (HyClone) and incubated in a humidified chamber (85% humidity) containing 5% CO_2 at 37 °C. On the morning of Aβ treatment, the cell culture medium was replaced with serum-free Dulbecco's modified Eagle's medium, and the cells were plated onto a 96-well, coated plate (Corning) at a final cell count of 20,000 cells/well. The cell viability was subsequently assessed using the MTT assay (see below).

MTT Assay—The toxic effects of spontaneous β-aggregation of Aβ on cell cultures were assessed. Solutions containing Aβ were prepared as described for the ThT assay, and then the samples were transferred immediately into wells containing the HEK293 cell (see "Cell Cultures"). After certain periods, MTT was added to each well, and the plate was kept in a CO_2 incubator for an additional 2 h. The cells were then lysed by the addition of a lysis solution (50% dimethylformamide, 20% SDS, pH 4.7) and were incubated overnight. The degree of MTT reduction in each sample was subsequently assessed by measuring absorption at 570 nm at 37 °C using a Bio Kinetics Reader EL340 (Bio-Tek Instruments). Background absorbance values, as assessed from cell-free wells, were subtracted from the absorption values of each test sample. The absorbances measured from three or six wells were averaged, and the percentage MTT reduction was calculated by dividing this average by the absorbance measured from a control sample without Aβ. By making three or six wells of each condition, their standard deviations were first calculated. They were then divided by the square root of n.

Immunoblotting Assay—Aβ sample was incubated for each time indicated at 37 °C as described above (see "ThT Assay"). Samples were collected and mixed with buffer containing glycerol but no reducing agents such as SDS or 2-mercaptoethanol. The formation of intermediate β-aggregates was assessed by 16.5% Tris-Tricine SDS-PAGE and immunoblotting using monoclonal antibody 4G8 (Signet Laboratories, Inc.), which recognizes residues 17–24 of Aβ.

Electron Microscopy—The ultrastructural characteristics of Aβ-aggregates were examined as follows. Aβ sample was incubated for indicated periods at 37 °C as described above (see "ThT Assay") and was mixed for 10 s every 20 min. 3 μl of each sample was applied to 300-mesh copper grids with formvar supporting membrane, blotted with filter paper, and stained with 1% (w/v) neutralized tungstophosphoric acid (Nacalai tesque, Inc., Kyoto, Japan). The specimens were examined on a LEO 912AB electron microscope (LEO, Oberkochen, Germany), at an accelerating voltage of 100 kV.

RESULTS

We first assessed the baseline kinetics of β-aggregation. The time course of β-aggregation was determined by incubating Aβ40 with ThT, a compound that fluoresces when specifically bound to β-sheet structures (16) (Fig. 1). Fluorometric measurements were carried out every 20 min for ~72 h at 37 °C. As expected (11–13), the β-aggregation kinetics was sigmoidal over the first 5 h of incubation (Fig. 1*A*). With increasing incubation, however, β-aggregation decreased slowly (Fig. 1*B*), decaying to an approximate asymptotic level of less than half the peak aggregation.

Because there are several competing hypotheses concerning the factor(s) associated with AD pathogenesis, it was of interest to analyze the toxicity, biochemical constituents, and structure of the aggregates during β-aggregation. At selected intervals during the first two days of incubation, Aβ/ThT samples were collected, transferred to HEK293 cell cultures grown in serum-free medium, and the toxicity of the Aβ/ThT solution was examined using the MTT assay, which assesses cell viability by measuring mitochondrial activity (17) (Fig. 1*C*). Even after only a short period of incubation, the β-aggregates that formed were highly toxic. With longer incubation, however, the β-aggregates were less toxic. We next determined the time course of the formation of different Aβ intermediates during the course of β-aggregation. The Aβ/ThT solutions were collected at selected times during aggregation and were analyzed by Western blot. Aliquots were applied to SDS-polyacrylamide gels and immunoblotted with an anti-Aβ antibody (Fig. 1*D*). Samples collected immediately after being incubated separated out as a thick band the size of the Aβ monomer and a thinner, less distinct band the size of the Aβ dimer, indicating that some dimerization had occurred almost immediately upon solubilization. After 2 h of incubation, the Aβ monomer band was less distinct, and an immunoreactive smear appeared, suggesting the formation of Aβ polymers. As incubation progressed, the amount of monomeric Aβ decreased. After extended incubation, we noticed increased staining at the bottom of the loading wells that presumably represented large aggregates that could not be resolved by the gel. The macromolecular structures of these various intermediates were examined using electron microscopy (Fig. 1, *E–H*). No distinguishable fiber-like structures were observed in samples collected soon after incubation began or in samples collected after 1 h of incubation. After 2 h of incubation, however, small oligomeric aggregates and long fibrils were observed (Fig. 1, *E* and *F*). The fibrils appeared to be comprised of two smaller filaments that were twisted around each other (Fig. 1*F*), but no further appreciable association between fibrils was observed. In contrast, after 4 h of incubation, the time point at which the greatest amount of β-aggregates formed (Fig. 1*C*), long fibers appeared to be gathered closely together in a net-like structure (Fig. 1*G*). After 27 h of incubation, Aβ fibers, aligned side by side and formed numerous fiber bundles (Fig. 1*H*). Interestingly, samples from this time period in the toxicity experiments were only moderately toxic; the most toxic Aβ-aggregates were those from the initial growth stage of fibrillogenesis. These findings prompted us to search for factors that cause an acute increase in the initial stage of β-aggregation.

Because individuals with familial Alzheimer's disease have larger proportions of Aβ42 compared with normal individuals (5–10), we examined the hypothesis that elevated levels of Aβ42 may play a role in the initial stage of β-aggregation. Thus, we measured the time course of β-aggregation formed by various ratios of Aβ40 and Aβ42 (Fig. 2*A*). Consistent with previous reports (11–13), incubation of Aβ42 alone showed signs of β-aggregation almost immediately after incubation began. After this initial increase, however, aggregation remained at a fairly constant, modest level without further significant increase. Pretreatment of Aβ42 with either HFIP or HFIP/NH_3 did not significantly alter the time course of β-aggregation. On the other hand, although the lag time until the start of β-aggregation of HFIP/NH_3-treated Aβ40 was much longer, the formation of β-aggregates increased to higher levels compared with that for Aβ42. Because longer lag time seemed more appropriate to examine the initial steps of aggregation in detail, HFIP/NH_3-treated Aβ40 was used in the rest of the experiments. When the proportion of Aβ42 was increased to the Aβ40:Aβ42 ratio of 10:1, β-aggregation kinetics systematically shifted to the left. Thus, Aβ42 accelerated the seeding or nucleation of Aβ40. When the proportion of Aβ40 to Aβ42 mimicked the proportion reported in some familial Alzheimer's disease mutants (*i.e.* Aβ40:Aβ42 ratio of 10:1) (10, 18), β-aggregation was further accelerated and also increased to a much higher level. Moreover, these Aβ42-induced aggregates were highly toxic when assessed with the MTT assay (Fig. 2*C*). At the end of the incubation period, the level of Aβ42-associated aggregation was lower than that of Aβ40 (Fig. 2*B*). Aggregates formed by Aβ42 alone were less toxic than aggregates formed from Aβ40 alone. The most toxic aggregates were in samples with the highest levels of aggregation (*i.e.* Aβ40:Aβ42 combined at a ratio of 10:1). Thus, it was of interest to examine the macromolecular structure of these aggregates (Fig. 2, *D–F*).

The approximate diameter of long fiber bundles formed by

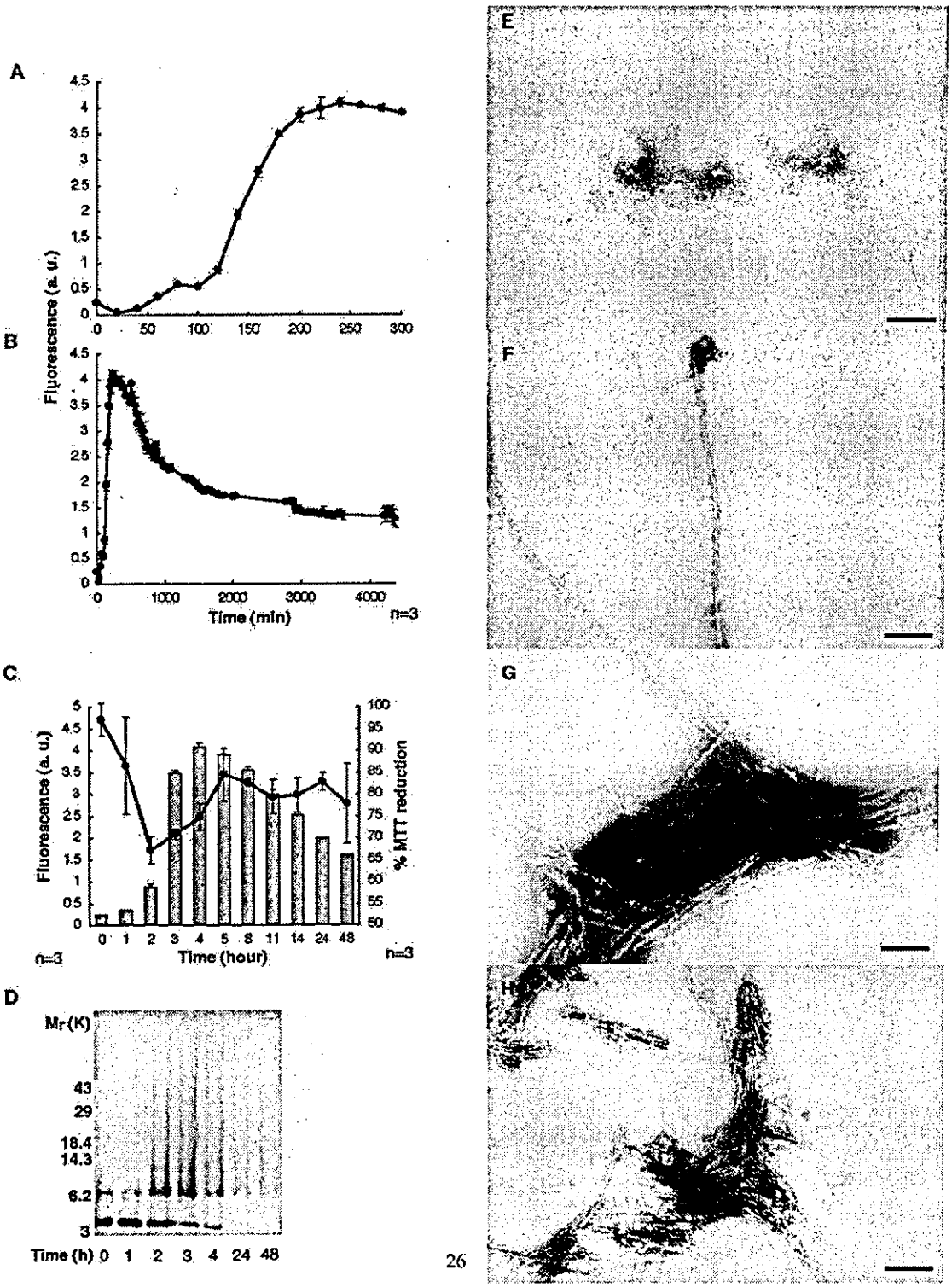

FIG. 1. **Time course of β-aggregation and toxicity of wild type Aβ40.** Aβ40 (5 μM) was pretreated with HFIP, a solvent that converts Aβ into a structural conformation normally found in cell membranes and was incubated with 10 μM ThT in 5 mM HEPES (pH 7.4) and 0.9% NaCl. *A*, early stage of β-aggregation, showing sigmoidal kinetics. *B*, entire time course, showing decay of β-aggregation as incubation progressed. *C*, toxicity of β-aggregates to cultured cells. At each time indicated, an Aβ/ThT sample was collected from the incubation well, and the well was rinsed with 50 μl of buffer. The rinsed solution was mixed with the Aβ/ThT sample. Five microliters of this mixture (*i.e.* 0.1 of the total volume of culture medium) was added to HEK293 cell cultures; the final concentration of Aβ was ~330 nM. The cells were incubated with this mixture for a total of 4 h; MTT was added to the cell cultures at the 2-h point to assess the degree of MTT reduction (*i.e.* cell viability). Fluorescence values (*bar graphs*) and % MTT values (*line graph*) are means ± S.E. throughout this report. *D*, Western blot showing the time course of β-aggregation. The formation of intermediate β-aggregates was also assessed by SDS-PAGE and immunoblotting using monoclonal antibody 4G8. *E–H*, electron photomicrographs showing macromolecular structures formed during the time course of β-aggregation. Five micromolar Aβ40 solution samples were incubated for 2 h (*E*), 2 h (*F*), 4 h (*G*), and 27 h (*H*). After incubation, 3 μl of Aβ40 solution was applied to Formvar-coated copper grids and negatively stained with neutralized tungstophosphoric acid. Magnification is 80,000; *scale bars* are 100 nm.

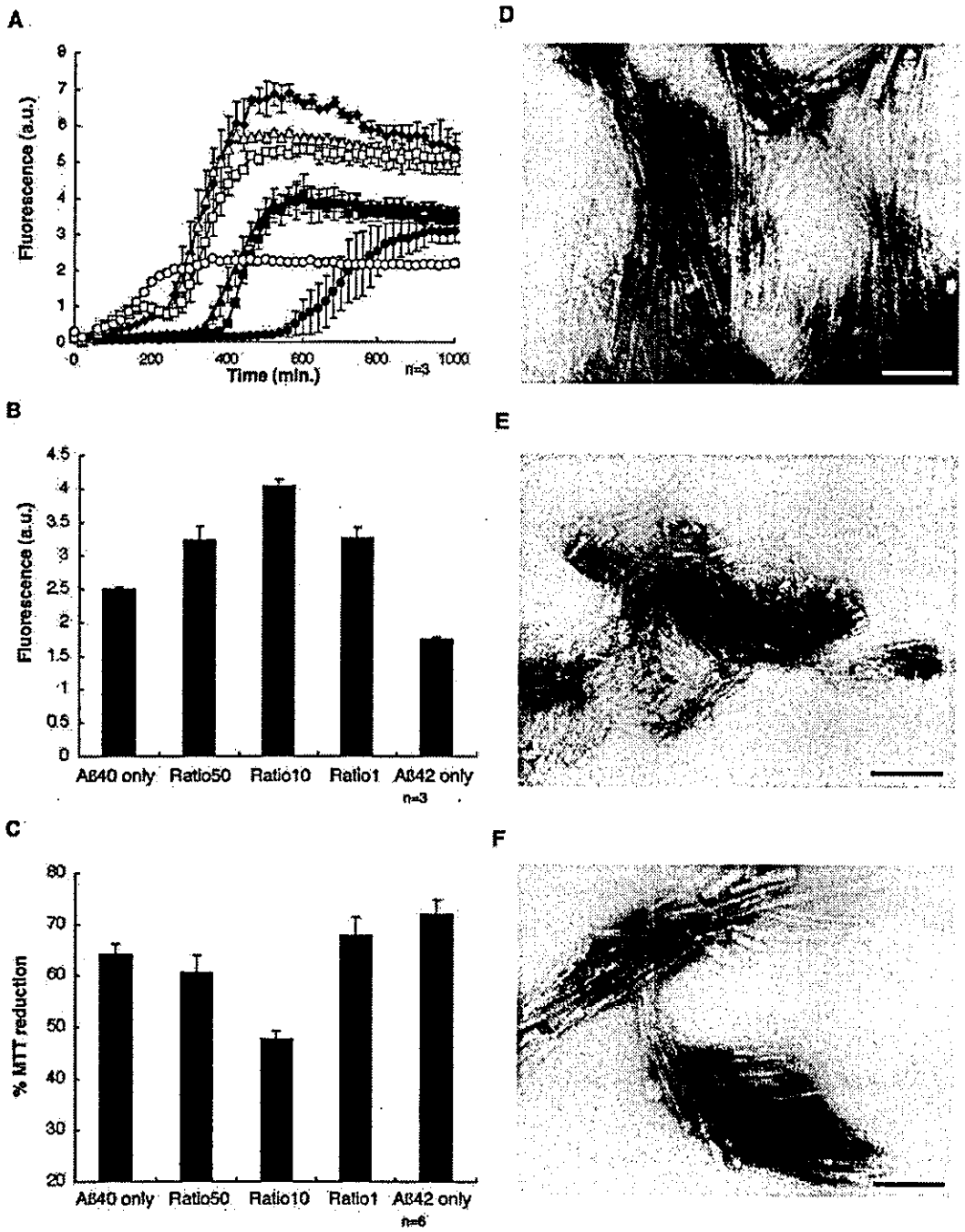

FIG. 2. **β-aggregation and toxicity by a mixture of wild type Aβ40 and Aβ42.** *A*, time course of β-aggregation was assessed using samples containing 5 μM ThT and various ratios of a mixture of Aβ40 and Aβ42 (total Aβ concentration: 5 μM). Aβ40 was pretreated with a 50% HFIP/14% NH_3 solution, and Aβ42 was pretreated with 100% HFIP. Solid (●) and open circles (○) are β-aggregation-induced by Aβ40 alone and Aβ42 alone, respectively. β-aggregation induced by different ratios of Aβ40 and Aβ42 are indicated as follows: 30:1 (■), 20:1 (▲), 10:1 (♦), 5:1 (△), and 3:1 (□). *B* and *C*, toxicity of β-aggregates formed by various combinations of Aβ40 and Aβ42. After 14 h of incubation, Aβ/ThT samples were collected. The incubation wells were rinsed with the same volume of buffer and then mixed with the Aβ/ThT samples. Part of this solution (*i.e.* 0.04 total volume of culture medium) was added to HEK293 cell cultures. *B*, *bar graphs* show the degree of β-aggregation in each sample immediately before the Aβ solution was added to the cultures. *C*, cell viability was assessed as described under "Experimental Procedures." *D–F*, electron photomicrographs showing aggregates formed following 5 days of incubation of 10 μM Aβ40 (*D*), 10 μM Aβ42 (*E*), and Aβ40:Aβ42 mixture (10:1) (*F*). The 5-day incubation period was long enough for β-aggregation to reach the final plateau level. The Aβ solution was prepared for electron microscopy examination as described under "Experimental Procedures." Magnification is 100,000; *scale bars* are 100 nm.

Aβ40 varied from 8 to 16 nm. On the other hand, closely associated fibers of aggregates formed by Aβ42 were shorter and had a maximum diameter of ~8 nm; thus, we provisionally called these fibers "protofibrils" (Fig. 2*E*). In samples containing Aβ40 and Aβ42 at a 10:1 ratio, aggregates formed fiber bundles that appeared shorter than extended Aβ40 fibers (compare Fig. 2, *F* and *D*). It is possible that, via the rapid formation of protofibrillar nuclei or seeds, Aβ42 enhanced β-aggregation as well as increased the toxicity of the Aβ40:Aβ42 mixture. However, our results thus far suggest that Aβ42 alone does not

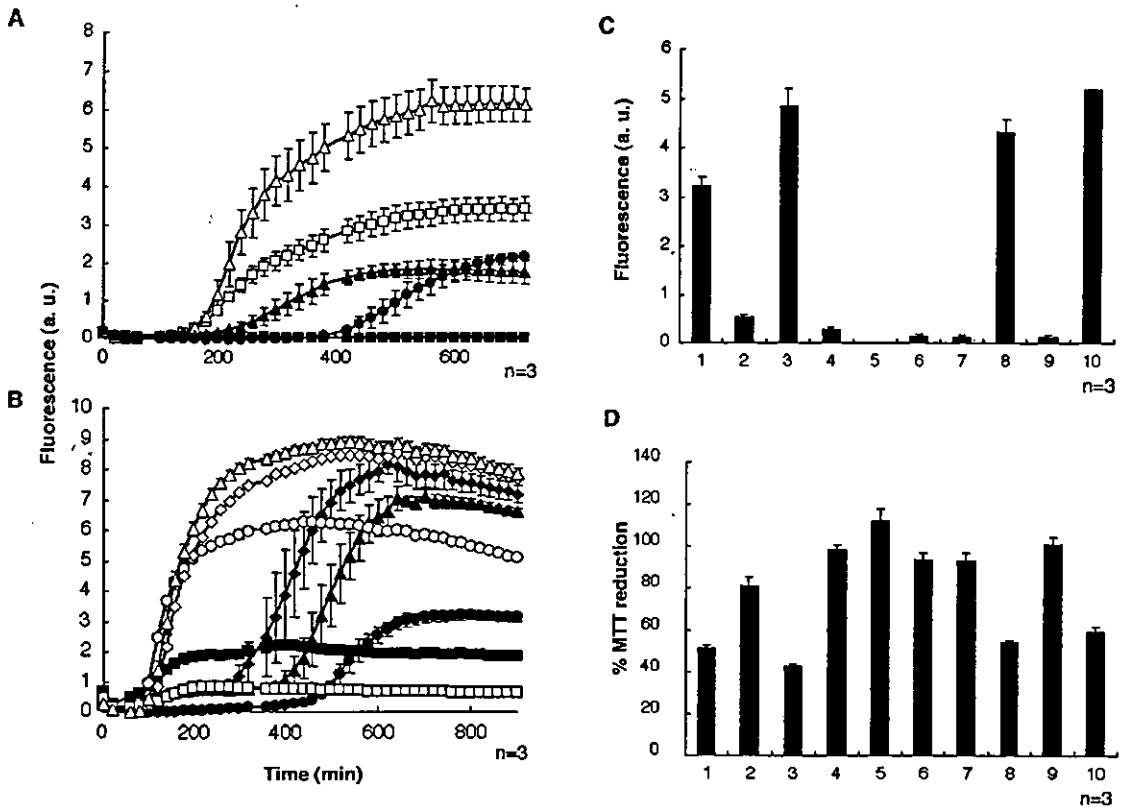

FIG. 3. **Effect on time-course of β-aggregation and toxicity by various Aβ variants having mutations in the N-terminal domain.** *A*, β-aggregation kinetics of wild type Aβ40 (●), Italian variant Aβ40 (E22K) (■), Dutch variant (E22Q) (▲). The final Aβ concentration for each of these samples was 5 μM. β-aggregation was also assessed for samples containing a 1:1 ratio of wild type Aβ40 and different Aβ variants as indicated: Italian (□), Dutch (●). *B*, impact of Aβ42 on aggregation. The following were assessed: wild type Aβ40 (●), wild type Aβ42 (■), wild type Aβ40 and Aβ42 (10:1) (♦), and wild type Aβ40 and Aβ42 (15:1) (▲). β-aggregation was also assessed for samples containing a 1:1 ratio of different wild type Aβ species and various Italian variant Aβ species as indicated: wild type Aβ40 and Italian Aβ40 (1:1) (○), wild type Aβ42 and Italian Aβ42 (1:1) (□), wild type Aβ40:Italian Aβ40 (1:1) and wild type Aβ42:Italian Aβ42 (1:1) at ratio of 10:1 (◇), and wild type Aβ40:Italian Aβ40 (1:1) and wild type Aβ42:Italian Aβ42 (1:1) at a ratio of 15:1 (△). For comparison, the mixture of wild type Aβ species was also measured. *C* and *D*, toxicity of aggregates formed by various Aβ variants. After 12 h of incubation, cell viability was assessed as described under "Experimental Procedures." *Bar graphs* in *panel C* represent the degree of β-aggregation; those in *panel D* represent the viability of the cells. *Numbers on the horizontal axis* represent the following: *1*, wild type Aβ40; *2*, wild type Aβ42; *3*, wild type Aβ40:wild type Aβ42 (10:1); *4*, Italian Aβ40; *5*, Italian Aβ42; *6*, Italian Aβ40:Italian Aβ42 (10:1); *7*, Italian Aβ40:Italian Aβ42 (15:1); *8*, wild type Aβ40:Italian Aβ40 (1:1); *9*, wild type Aβ42:Italian Aβ42 (1:1); and *10*, wild Aβ40:Italian Aβ40 (1:1) and wild type Aβ42:Italian Aβ42 (1:1) at a ratio of 15:1.

cause large elongation. In the next set of experiments, we sought to determine whether certain other factors affect the elongation step of β-aggregate formation. As previously suggested, the hydrophobic nature of the Aβ42 C terminus is critical for accelerating the seeding process (11–13). Thus, if the C terminus is related to seeding, we hypothesized that the N terminus of Aβ may be related to elongation.

To test this hypothesis, we assessed the β-aggregation kinetics of several Aβ40 peptides with pathogenic mutations in the N-terminal domain, Italian variant (E22K) and Dutch variant (E22Q). Previously, such substitutions were suggested to affect the intersheet stacking between β-sheets (19–21). We compared the β-aggregation time courses of wild type Aβ40 (E22), Italian variant (E22K), Dutch variant (E22Q), and their mixtures (Fig. 3*A*) (20, 21). None of the variants by themselves showed significantly higher levels of β-aggregation compared with that of the wild type. Indeed, Italian variant (E22K) showed undetectable β-aggregation. However, only when the Italian or Dutch variants were mixed with wild type Aβ40 in a 1:1 ratio did β-aggregation increase significantly during the early stage of elongation. Although the Dutch variant alone formed β-aggregates faster than wild type Aβ40, the mixing of the two induced and enhanced elongation. Although β-aggregation by the Italian variant and wild type Aβ40 mixture was faster and more robust compared with that of the wild type alone, β-aggregation by the Italian variant alone was undetectable. Clearly, the interactions between hydrophilic residues in the N-terminal domain play an important role in elongation under our experimental conditions.

As before, we assessed the impact of Aβ42 on β-aggregation, this time in ratios reported for wild type Aβ40 and Italian variant Aβ40 *in vitro* (22) (Fig. 3*B*). When wild type or variant Aβ42 was added to the wild type Aβ40/Italian Aβ40 sample, an even larger elongation was observed compared with that when Aβ42 was absent (Fig. 3*C*). This combination was very toxic as well (Fig. 3*D*). The most probable reason to explain the difference between the time courses of aggregation of a mixture containing wild type Aβ40 and Italian Aβ40 in Fig. 3, *A* and *B* would be the difference between two lots of Italian Aβ40 peptides, one lot from American Peptides (Fig. 3*A*) and the other from RIKEN BSI (Fig. 3, *B–D* and Fig. 4*B*). Nonetheless, one is tempted to draw conclusions about phenotypes from these *in vitro* results. The differences in nucleation and elongation of β-aggregation resulting from different Aβ combinations do not completely explain differences in the pathological features of these mutations that show altered Aβ40:Aβ42 ratios and Aβ sequence mutations. However, because conditions that mimic these pathogenic mutations both induce and accelerate β-ag-

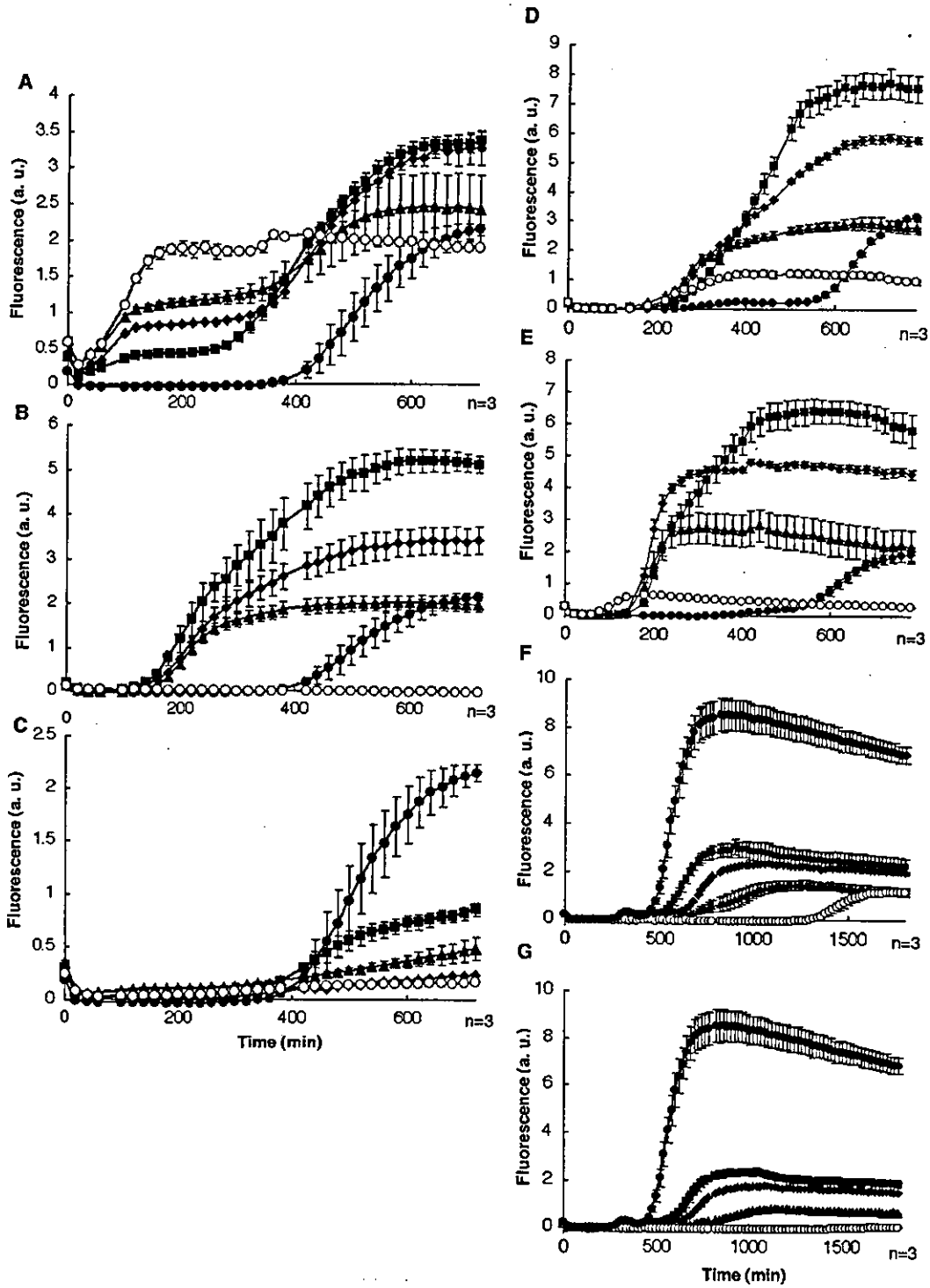

FIG. 4. **Respective roles of the Aβ42 C terminus and Aβ40 N terminus in β-aggregation.** *A*, five samples composed of different ratios of wild type Aβ40 and wild type Aβ42, as indicated, were incubated and β-aggregation was assessed: 5:0 (●), 3.5:1.5 (■), 2.5:2.5 (♦), 1.5:3.5 (▲), and 0:5 (○). The total concentration of Aβ in these samples was 5 μM. *B*, β-aggregation kinetics of Aβ mixtures composed of wild type Aβ40 and Italian Aβ40 at the indicated ratios: 5:0 (●), 3.5:1.5 (■), 2.5:2.5 (♦), 1.5:3.5 (▲), and 0:5 (○). *C*, β-aggregation kinetics of Aβ mixtures composed of wild type Aβ40 and Italian Aβ42 at the indicated ratios: 5:0 (●), 3.5:1.5 (■), 2.5:2.5, (▲) 1.5:3.5 (♦), and 0:5 (○). *D–G*, β-aggregation kinetics of Aβ mixtures composed of wild type Aβ40 and four non-pathogenic mutants of position 22 (see "Experimental Procedures") at the indicated ratios: 5:0 (●), 3.5:1.5 (■), 2.5:2.5 (♦), 1.5:3.5 (▲), and 0:5 (○). *D*, wild type Aβ40:mutant Aβ40 (E22R). *E*, wild type Aβ40:mutant Aβ40 (E22shortK). *F*, wild type Aβ40:mutant Aβ40 (E22D). *G*, wild type Aβ40:mutant Aβ40 (E22longE).

gregation, as well as elevate toxicity (Fig. 3, *C* and *D*), the acute increase in β-aggregation at the initial stage is consistent with pathogenesis of amyloid-related disorders.

Our results thus far clearly hint that particular proportions of Aβ40 and Aβ42 either enhance or retard nucleation and elongation. Our findings are also consistent with previous stud-

ies showing that the accelerating effect of Aβ42 resides in the hydrophobicity of its C terminus (11–13), and the hydrophilic side chains in the N terminus most probably have an effect on intersheet stacking (19). In this last set of experiments, because overall β-aggregation depends on the relationship of factors that affect nucleation and elongation, we took a closer look at the respective role(s) of such factors, such as the Aβ42 C terminus and Aβ40 N terminus, in β-aggregation. To determine whether disproportionately greater concentrations of Aβ42 affect nucleation, we first assessed the aggregation kinetics of samples containing broader ratios of Aβ40:Aβ42. As seen in Fig. 2, greater proportions of wild type Aβ42 accelerated the seeding of Aβ40 (Fig. 4*A*). In terms of the elongation process, however, the proportion of Aβ42 appeared to have an inverse effect. In samples containing larger proportions of Aβ42 than Aβ40, the overall level of β-aggregation was lower (Fig. 4*A*). On the other hand, although Italian variant Aβ40 induced the seeding of wild type Aβ40 less effectively compared with that by wild type Aβ42, it effectively induced the elongation of aggregates formed by wild type Aβ40 (Fig. 4*B*).

As mentioned, the induction effect of wild Aβ42 is related to the hydrophobic nature of its C-terminal, resulting in β-sheet formation (11–13). On the other hand, the effect of Italian variant Aβ40 is due to the substitution of a negatively charged Glu at position 22 to a positively charged Lys. This likely induces β-aggregation through electrostatic interaction of side chains, thus promoting intersheet stacking (19) and elongation. Because this is an interaction between paired β-sheets having oppositely charged side chains, Italian variant Aβ40 does not aggregate by itself. This notion was further supported by experiments mixing four kinds of non-pathogenic mutants at position 22 with wild type Aβ40 (Fig. 4, *D–G*). Although the degree of induction effect was slightly different, two mutant Aβ40s having positively charged Arg and shortK (see "Experimental Procedures") induced the elongation of wild type Aβ40 in a manner similar to the Italian variant (E22K) (Fig. 4, *D*, *E*, and *B*). To examine the effect of size of side chains at position 22, we also tested two other mutants with negatively charged Asp and longE (see "Experimental Procedures"). Both mutants by themselves showed lower levels of β-aggregation than wild type Aβ40 (Fig. 4, *F* and *G*). Moreover, as the proportion of E22D and E22longE was increased, the β-aggregation was decreased in a dose-dependent manner, suggesting the importance of size of side chains in β-aggregation. In contrast, although all the mutants with positively charged residue at 22 (E22K, E22R, and E22shortK) by themselves also had lower β-aggregation level than wild type, when their small proportions were mixed with wild type, β-aggregation was significantly elevated. These results suggest the important role of electrostatic interactions of side chains in the β- aggregation process.

Substantial induction effects by both wild Aβ42 and Italian variant Aβ40 on the overall β-aggregation of wild Aβ40 were observed when the proportion of inducers was smaller than wild Aβ40. Because overall β-aggregation depends on both β-sheet formation (*i.e.* nucleation) and intersheet stacking (*i.e.* elongation), specific balance between these interactions determines the formation of fast and induced β-aggregation that leads to toxic activity. The importance of such balance is underscored by our finding that Italian variant Aβ42 suppressed the aggregation of wild type Aβ40 at all ratios tested (Fig. 4*C*). This is because the hydrophobic effect at the C terminus and electrostatic interactions between side chains are physically opposed. Only when they balance at the certain composition of Aβ peptides are toxic β-aggregates formed.

DISCUSSION

There is tremendous evidence that supports a single hypothesis for the pathogenesis of AD. This so-called "amyloid hypothesis" suggests that the process of Aβ deposition is intimately connected to the initiation of AD pathogenesis and that all other features of the disease are secondary to this initiation (23, 24). A recent, novel suggestion relating to this hypothesis is that oligomeric aggregates of Aβ peptides are the forms that generate neurotoxicity (25, 26). The aggregation kinetics presented in Fig. 1 show that initially formed aggregates are indeed more toxic than fiber bundles formed after a long incubation. However, one cannot conclude from these observations that deposited amyloids or bundles of fibers are innocuous but suggest that they are possibly less neurotoxic than initially formed Aβ-aggregates.

Mixing Aβ40 and Aβ42 at specific ratios induced and accelerated β-aggregation. These results suggest that particular ratios of Aβ species are very important for the toxic β-aggregation process and perhaps in AD pathogenesis. However, elevated ratios of Aβ42/40 have not been observed in the media collected from cells transfected with several intra-Aβ mutations, including the Dutch and Italian cases (22). The predominant increase of β-aggregation observed by mixing both wild type and Italian variant Aβ suggests that elongation is largely dependent on interactions between the N-terminal side chains of β-sheets, which are nucleated by hydrophobic interactions of C-terminal regions. Hydrophobic residues in the N-terminal domain may also induce nucleation or elongation by an entropically driven process, whereas other polar or charged side chains will interact more directly with each other. The latter type of interaction is hydrophilic and thus is generally known to be weaker in stabilizing proteins. Because these two types of interactions usually repel each other in a manner similar to oil and water, Aβ compositions that balance these interactions in a specific way determine whether the formation of toxic β-aggregates proceeds effectively. This is relevant to the possible mechanism of Aβ toxicity. One idea is that Aβ-aggregates penetrate the membrane structure either extracellularly or intracellularly (27). β-sheeted Aβ-aggregates formed under conditions in which polar-nonpolar interactions are balanced in a specific way would make an alignment of charged residues that perhaps disrupt functions of the cell membrane. This is consistent with a recent finding that non-fibrillar, ThT-*positive* aggregates (*i.e.* aggregates of β-sheets) of a wide range of misfolded proteins exhibit similar toxicity to that shown in the present study (28).

Acknowledgments—We thank Y. Tatebayashi and T. Miyasaka for critical advice, A. Sekimata-Murakami for technical assistance, and N. Hirotani for synthesizing peptides.

REFERENCES

1. Glenner, G. G., and Wong, C. W. (1984) *Biochem. Biophys. Res. Commun.* **120**, 885–890
2. Masters, C. L., Simms, G., Weinman, N. A., Multhaup, G., McDonald, B. L., and Beyreuther, K. (1985) *Proc. Natl. Acad. Sci. U. S. A.* **82**, 4245–4249
3. De Strooper, B., Saftig, P., Craessaerts, K., Vanderstichele, H., Guhde, G., Annaert, W., Von Figura, K., and Van Leuven, F. (1998) *Nature* **391**, 387–390
4. Vassar, R., Bennett, B. D., Babu-Khan, S., Kahn, S., Mendiaz, E. A., Denis, P., Teplow, D. B., Ross, S., Amarante, P., Loeloff, R., Luo, Y., Fisher, S., Fuller, J., Edenson, S., Lile, J., Jarosinski, M. A., Biere, A. L., Curran, E., Burgess, T., Louis, J. C., Collins, F., Treanor, J., Rogers, G., and Citron, M. (1999) *Science* **286**, 735–741
5. Goate, A., Chartier-Harlin, M. C., Mullan, M., Brown, J., Crawford, F., Fidani, L., Giuffra, L., Haynes, A., Irving, N., James, L., Mant, R., Newton, P., Rooke, K., Roques, P., Talbot, C., Pericak-Vance, M., Roses, A., Williamson, R., Rossor, M., Owen, M., and Hardy, J. (1991) *Nature* **349**, 704–706
6. Mullan, M., Crawford, F., Axelman, K., Houlden, H., Lilius, L., Winblad, B., and Lannfelt, L. (1992) *Nat. Genet.* **1**, 345–347
7. Hardy, J. (1992) *Nat. Genet.* **1**, 233–234
8. Hendriks, L., van Duijn, C. M., Cras, P., Cruts, M., Van Hul, W., van Harskamp, F., Warren, A., McInnis, M. G., Antonarakis, S. E., Martin, J. J., Hofman, A., and Van Broeckhoven, C. (1992) *Nat. Genet.* **1**, 218–221

9. Wisniewski, T., Ghiso, J., and Frangione, B. (1991) *Biochem. Biophys. Res. Commun.* **179**, 1247–1254
10. Scheuner, D., Eckman, C., Jensen, M., Song, X., Citron, M., Suzuki, N., Bird, T. D., Hardy, J., Hutton, M., Kukull, W., Larson, E., Levy-Lahad, E., Viitanen, M., Peskind, E., Poorkaj, P., Schellenberg, G., Tanzi, R., Wasco, W., Lannfelt, L., Selkoe, D., and Younkin, S. (1996) *Nature Med.* **2**, 864–870
11. Barrow, C. J., and Zagorski, M. G. (1991) *Science* **253**, 179–182
12. Burdick, D., Soreghan, B., Kwon, M., Kosmoski, J., Knauer, M., Henschen, A., Yates, J., Cotman, C., and Glabe, C. (1991) *J. Biol. Chem.* **267**, 546–554
13. Jarrett, J. T., and Lansbury, P. T., Jr. (1993) *Cell* **73**, 1055–1058
14. Olson, M. I., and Shaw, C. M. (1969) *Brain* **92**, 147–156
15. Selkoe, D. J. (2001) *Physiol. Rev.* **81**, 741–766
16. LeVine, H., III, (1993) *Protein Sci.* **2**, 404–410
17. Hansen, M. B., Nielsen, S. E., and Berg, K. (1989) *J. Immunol. Methods* **119**, 203–210
18. Suzuki, N., Cheung, T. T., Cai, X. D., Odaka, A., Otvos, L., Jr., Eckman, C., Golde, T. E., and Younkin, S. G. (1994) *Science* **264**, 1336–1340
19. Kirschner, D. A., Inouye, H., Duffy, L. K., Sinclair, A., Lind, M., and Selkoe, D. J. (1987) *Proc. Natl. Acad. Sci. U. S. A.* **84**, 6953–6957
20. Tagliavini, F., Rossi, G., Padovani, A., Magoni, M., Andora, G., Sgarzi, M., Bizzi, A., Savoiardo, M., Carella, F., Morbin, M., Giaccone, G., and Bugiani, O. (1999) *Alzheimer's. Rep.* **2**, 23 (abstr.)
21. Levy, E., Carman, M. D., Fernandez-Madrid, I. J., Power, M. D., Lieberburg, I., van Duinen, S. G., Bots, G. T., Luyendijk, W., and Frangione, B. (1990) *Science* **248**, 1124–1126
22. Nilsberth, C., Westlind-Danielsson, A., Eckman, C. B., Condron, M. M., Axelman, K., Forsell, C., Stenh, C., Luthman, J., Teplow, D. B., Younkin, S. G., Naslund, J., and Lannfelt, L. (2001) *Nat. Neurosci.* **4**, 887–893
23. Taylor, J. P., Hardy, J., and Fischbeck, K. H. (2002) *Science* **296**, 1991–1995
24. Hardy, J., and Selkoe, D. J. (2002) *Science* **297**, 353–356
25. Walsh, D. M., Klyubin, I., Fadeeva, J. V., Cullen, W. K., Anwyl, R., Wolfe, M. S., Rowan, M. J., and Selkoe, D. J. (2002) *Nature* **416**, 535–539
26. Kirkitadze, M. D., Condron, M. M., and Teplow, D. B. (2001) *J. Mol. Biol.* **312**, 1103–1119
27. Lashuel, H. A., Hartley, D., Petre, B. M., Walz, T., and Lansbury, P. T., Jr. (2002) *Nature* **418**, 291
28. Bucciantini, M., Giannoni, E., Chiti, F., Baroni, F., Formigli, L., Zurdo, J., Taddei, N., Ramponi, G., Dobson, C. M., and Stefani, M. (2002) *Nature* **416**, 507–511

Journal of Neurochemistry, 2003, 87, 172–181 doi:10.1046/j.1471-4159.2003.01976.x

Potent anti-amyloidogenic and fibril-destabilizing effects of polyphenols *in vitro*: implications for the prevention and therapeutics of Alzheimer's disease

Kenjiro Ono,* Yuji Yoshiike,† Akihiko Takashima,† Kazuhiro Hasegawa,‡ Hironobu Naiki‡ and Masahito Yamada*

**Department of Neurology and Neurobiology of Aging, Kanazawa University Graduate School of Medical Science, Kanazawa 920–8640, Japan*

†Laboratory for Alzheimer's Disease, Brain Science Institute, RIKEN, Wako, Saitama 351–0198, Japan

‡Department of Pathology, Fukui Medical University, Fukui 910–1193, and CREST of Japan Science and Technology Corporation, Japan

Abstract

Cerebral deposition of amyloid β-peptide (Aβ) in the brain is an invariant feature of Alzheimer's disease (AD). A consistent protective effect of wine consumption on AD has been documented by epidemiological studies. In the present study, we used fluorescence spectroscopy with thioflavin T and electron microscopy to examine the effects of wine-related polyphenols (myricetin, morin, quercetin, kaempferol (+)-catechin and (–)-epicatechin) on the formation, extension, and destabilization of β-amyloid fibrils (fAβ) at pH 7.5 at 37°C *in vitro*. All examined polyphenols dose-dependently inhibited formation of fAβ from fresh Aβ(1–40) and Aβ(1–42), as well as their extension. Moreover, these polyphenols dose-dependently destabilized preformed fAβs. The overall activity of the molecules examined was in the order of: myricetin = morin = quercetin > kaempferol > (+)-catechin = (–)-epicatechin. The effective concentrations (EC_{50}) of myricetin, morin and quercetin for the formation, extension and destabilization of fAβs were in the order of 0.1–1 μM. In cell culture experiments, myricetin-treated fAβ were suggested to be less toxic than intact fAβ, as demonstrated by 3-[4,5-dimethylthiazol-2-yl]-2,5-diphenyltetrazolium bromide assay. Although the mechanisms by which these polyphenols inhibit fAβ formation from Aβ, and destabilize pre-formed fAβ *in vitro* are still unclear, polyphenols could be a key molecule for the development of preventives and therapeutics for AD.

Keywords: Alzheimer's disease, β-amyloid fibrils, cytotoxicity, electron microscopy, polyphenols, thioflavin T.

J. Neurochem. (2003) **87**, 172–181.

Alzheimer's disease (AD) is characterized by the abundance of intraneuronal neurofibrillary tangles and the extracellular deposition of the amyloid β-peptide (Aβ) as amyloid plaques and vascular amyloid (Selkoe 2001). Despite recent progress in the symptomatic therapy with cholinergic drugs (Doody *et al.* 2001), an effective therapeutic approach that interferes directly with the neurodegenerative process in AD, especially the accumulation of Aβ in the CNS is eagerly awaited. Recently, immunization with Aβ (Schenk *et al.* 1999) and treatment with a copper-zinc chelator (Cherny *et al.* 2001) were reported to attenuate the accumulation of Aβ in AD transgenic mice.

The notion that red wine may have potential health benefits initially received a great deal of attention following

Received May 5, 2003; revised manuscript received June 19, 2003; accepted June 20, 2003.

Address correspondence and reprint requests to Dr M. Yamada, Department of Neurology & Neurobiology of Aging, Kanazawa University Graduate School of Medical Science, Kanazawa 920–8640, Japan. E-mail: m-yamada@med.kanazawa-u.ac.jp or Dr H. Naiki at Department of Pathology, Fukui Medical University, Fukui 910–1193, Japan. E-mail: naiki@fmsrsa.fukui-med.ac.jp

Abbreviations used: Aβ, amyloid β-peptide; AD, Alzheimer's disease; apoE, apolipoprotein E; BBB, blood–brain barrier; Cat, (+)-catechin; DMEM, Dulbecco's modified Eagle's medium; DMSO, dimethyl sulfoxide; EC_{50}, effective concentrations at 50% value; epi-Cat, (–)-epicatechin; fAβ, β-amyloid fibrils; HEK, human embryonic kidney; Kmp, kaempferol; Mor, morin; MTT, 3-[4,5-dimethylthiazol-2-yl]-2,5-diphenyltetrazolium bromide; Myr, myricetin; NDGA, nordihydroguaiaretic acid; Qur, quercetin; RIF, rifampicin; TC, tetracycline; ThT, thioflavin T.

the report that moderate wine consumption was linked to a lower incidence of coronary heart disease, an effect known as the French paradox (Renaud and de Lorgeril 1992). In addition to the purported cardioprotective effects of red wine, French and Danish epidemiological studies have suggested that moderate wine drinking may protect against AD (Dartigues and Orgogozo 1993; Dorozynski 1997; Orgogozo *et al.* 1997; Truelsen *et al.* 2002). The role of ethanol in the protective properties of red wine is however, uncertain (Soleas *et al.* 1997; van Golde *et al.* 1999). In addition to ethanol, red wine contains a broad range of polyphenols that are present in the skin and seeds of grapes (Hertog *et al.* 1993; Celotti *et al.* 1996; Goldberg *et al.* 1996; Sato *et al.* 1997; Soleas *et al.* 1997). Recently, several studies have suggested that many kinds of natural polyphenols may have neuroprotective effects both *in vivo* and *in vitro*, possibly due to their abilities to scavenge reactive oxygen species (Inanami *et al.* 1998; Shutenko *et al.* 1999; Bastianetto *et al.* 2000; Virgili and Contestabile 2000; Choi *et al.* 2001; Levites *et al.* 2001). Choi *et al.* (2001) demonstrated that green tea polyphenol (–)-epigallocatechin gallate attenuates β-amyloid-induced neurotoxicity in cultured hippocampal neurons through scavenging reactive oxygen species. However, few reports that describe the effects of polyphenols on the formation and destabilization of Alzheimer's β-amyloid fibrils (fAβ) *in vitro* have thus far been available.

Using a nucleation-dependent polymerization model to explain the mechanism of fAβ formation *in vitro* (Jarrett and Lansbury 1993; Lomakin *et al.* 1997; Naiki *et al.* 1997; Naiki and Gejyo 1999), we previously reported that nordihydroguaiaretic acid (NDGA) and rifampicin (RIF) inhibit fAβ formation from Aβ and fAβ extension dose-dependently *in vitro* (Naiki *et al.* 1998). Moreover, we reported that NDGA also destabilizes fAβ(1–40) and fAβ(1–42) in a concentration-dependent manner within a few hours at pH 7.5 at 37°C, based on fluorescence spectroscopic analysis with thioflavin T (ThT) and electron microscopic studies (Ono *et al.* 2002b). The activity of NDGA to destabilize fAβ(1–40) and fAβ(1–42) in comparison with other molecules reported to inhibit fAβ formation from Aβ and/or to destabilize pre-formed fAβ both *in vivo* and *in vitro* was in the order of: NDGA > > RIF = tetracycline (TC) > poly(vinylsulfonic acid, sodium salt) = 1,3-propanedisulfonic acid, disodium salt > β-sheet breaker peptide (iAβ5) > nicotine (Ono *et al.* 2002a; Ono *et al.* 2002b). Moreover, in cell culture experiments, fAβ treated by NDGA was significantly less toxic than intact fAβ (Ono *et al.* 2002b).

Using fluorescence spectroscopy with ThT and electron microscopy, we examined the effects of the major natural polyphenols on the formation, extension, and destabilization of fAβ(1–40) and fAβ(1–42) at pH 7.5 and 37°C *in vitro*. We also compared the cytotoxicity of myricetin (Myr)-treated fAβ with that of intact fAβ, by measuring the reducing rate of 3-[4,5-dimethylthiazol-2-yl]-2,5-diphenyltetrazolium bromide (MTT).

Experimental procedures

Preparation of Aβ and fAβ solutions

Aβ(1–40) (a trifluoroacetate salt, lot number 520130, Peptide Institute Inc., Osaka, Japan) and Aβ(1–42) (a trifluoroacetate salt, lot number 520625, Peptide Institute Inc., Osaka, Japan) were dissolved by brief vortexing in 0.02% ammonia solution at a concentration of 500 μM (2.2 mg/mL) and 250 μM, respectively, in a 4°C room and stored at −80°C before assaying (fresh Aβ(1–40) and Aβ(1–42) solutions). fAβ(1–40) and fAβ(1–42) were formed from the fresh Aβ(1–40) and Aβ(1–42) solutions, respectively, sonicated, and stored at 4°C as described in Hasegawa *et al.* (1999).

Fresh, non-aggregated fAβ(1–40) and fAβ(1–42) were obtained by extending sonicated fAβ(1–40) or fAβ(1–42) with fresh Aβ (1–40) or Aβ(1–42) solutions, respectively, just before the destabilization reaction (Ono *et al.* 2002a; Ono *et al.* 2002b). The reaction mixture was 600 μL and contained 10 μg/mL (2.3 μM) fAβ(1–40) or fAβ(1–42), 50 μM Aβ(1–40) or Aβ(1–42), 50 mM phosphate buffer, pH 7.5, and 100 mM NaCl. After incubation at 37°C for 3–6 h under non-agitated conditions, the extension reaction proceeded to equilibrium as measured by the fluorescence of ThT. In the following experiment, the concentration of fAβ(1–40) and fAβ (1–42) in the final reaction mixture was regarded as 50 μM.

Fluorescence spectroscopy, electron microscopy, and polarized light microscopy

A fluorescence spectroscopic study was performed as described by Naiki and Nakakuki (1996) on a Hitachi F-2500 fluorescence spectrophotometer (Tokyo, Japan). Optimum fluorescence measurements of fAβ(1–40) and fAβ(1–42) were obtained at the excitation and emission wavelengths of 445 and 490 nm, respectively, with the reaction mixture containing 5 μM ThT (Wako Pure Chemical Industries Ltd, Osaka, Japan) and 50 mM of glycine-NaOH buffer, pH 8.5. An electron microscopic study and polarized light microscopic study of the reaction mixtures were performed as described elsewhere (Hasegawa *et al.* 1999).

Polymerization assay

Polymerization assay was performed as described in Naiki *et al.* (1998). The reaction mixture contained 50 μM Aβ(1–40), or 25 or 50 μM Aβ(1–42), 0 or 10 μg/mL fAβ(1–40) or fAβ(1–42), 0, 0.01, 0.1, 1, 10, or 50 μM NDGA or polyphenols (Myr, morin (Mor), quercetin (Qur), kaempferol (Kmp) (+)-catechin (Cat) (–)-epicatechin (epi-Cat) [Sigma Chemical Co., St. Louis, MO, USA], 1% dimethyl sulfoxide (DMSO) (Nacalai Tesque, Inc., Kyoto, Japan), 50 mM phosphate buffer, pH 7.5, and 100 mM NaCl. NDGA and polyphenols were first dissolved in DMSO at concentrations of 1, 10, 100 μM, 1 and 5 mM, then added to the reaction mixture to make the final concentrations 0.01, 0.1, 1, 10 and 50 μM, respectively.

Thirty μL aliquots of the mixture were put into oil-free PCR tubes (size: 0.5 mL, code number: 9046; Takara Shuzo Co. Ltd, Otsu, Japan). The reaction tubes were then put into a DNA thermal cycler (PJ480; Perkin Elmer Cetus, Emeryville, CA, USA). The plate temperature was elevated at maximal speed, starting at 4°C, to 37°C. Incubation times ranged from between 0 and 8 days (as